JAMES | Journal of Advances in Modeling Earth Systems

RESEARCH ARTICLE
10.1029/2024MS004593

A Model for Regional-Scale Water Erosion and Sediment Transport and Its Application to the Yellow River Basin

Cong Jiang[1,2], Eric J. R. Parteli[3], and Yaping Shao[1]

[1]Institute for Geophysics and Meteorology, University of Cologne, Cologne, Germany, [2]Department of Ecohydrology and Biogeochemistry, Leibniz Institute of Freshwater Ecology and Inland Fisheries, Berlin, Germany, [3]Faculty of Physics, University of Duisburg-Essen, Duisburg, Germany

Key Points:

- Development of the Atmospheric and Hydrological-Sediment Modeling System for regional water erosion and sediment transport
- Gully erosion plays a crucial role in sediment supply on the Chinese Loess Plateau
- Global warming increases sediment discharge and enhanced irrigation increases sediment deposition in the Yellow River Basin

Supporting Information:

Supporting Information may be found in the online version of this article.

Correspondence to:

C. Jiang,
cong.jiang@igb-berlin.de

Citation:

Jiang, C., Parteli, E. J. R., & Shao, Y. (2025). A model for regional-scale water erosion and sediment transport and its application to the yellow river basin. *Journal of Advances in Modeling Earth Systems*, *17*, e2024MS004593. https://doi.org/10.1029/2024MS004593

Received 23 JUL 2024
Accepted 8 APR 2025

Correction added on 11 JUN 2025, after first online publication: Projekt DEAL funding statement has been added.

Author Contributions:

Conceptualization: Cong Jiang, Eric J. R. Parteli, Yaping Shao
Formal analysis: Cong Jiang
Funding acquisition: Eric J. R. Parteli, Yaping Shao
Investigation: Cong Jiang
Methodology: Cong Jiang
Project administration: Eric J. R. Parteli, Yaping Shao
Resources: Yaping Shao
Software: Cong Jiang

Abstract On catchment scales, sediment discharge depends on both sediment transport capacity and sediment availability. The quantification of sediment discharge at the regional scales is important but is rarely adequately represented in regional hydrological models. Here, we introduce a regional water erosion and sediment transport model, Atmospheric and Hydrological-Sediment Modeling System (AHMS-SED). This model integrates the Atmospheric and Hydrological Modeling System (AHMS) with the improved CASCade 2-Dimensional SEDiment (CASC2D-SED) model and incorporates gully erosion as a significant factor affecting sediment supply. A gully area index is introduced to quantify the fraction of the gully area and the enhancement of water erosion induced by concentrated flow in gullies. We use the AHMS-SED to simulate the sediment processes in the Yellow River Basin from 1979 to 1987 at a 20 km resolution. We find quantitative agreement between the observations and model predictions for monthly sediment fluxes at five major hydrological stations along the Yellow River, with excellent performance metrics (modified Kling-Gupta efficiency = 0.90, Nash–Sutcliffe model efficiency coefficient = 0.81) at the basin outlet. The results demonstrate the strong performance of the AHMS-SED and the robustness of the sediment supply estimates. We also use AHMS-SED to investigate how changes in climate and human activities affect sediment discharge in the Yellow River. The model shows that halving precipitation intensity substantially reduces sediment discharge, halving precipitation amount reduces it by 60%, and doubling irrigation reduces it by 10%.

Plain Language Summary To know how sediment moves through river systems in large catchments is vital for addressing challenges in agriculture, hydrology, ecology, and geomorphology. However, existing regional hydrological models often do not represent processes like gully erosion well, which is essential to sediment discharge. We present here a new computer model, the Atmospheric and Hydrological-Sediment Modeling System (AHMS-SED), that combines the Atmospheric and Hydrological Modeling System with the modified CASCade 2-Dimensional SEDiment (CASC2D-SED) model, accounting for gully erosion. We use the AHMS-SED to simulate water erosion and sediment processes in the Yellow River Basin from 1979 to 1987 at a 20 km resolution. The model shows good agreement with observed data, with excellent performance metrics (modified Kling-Gupta efficiency = 0.90, Nash–Sutcliffe model efficiency coefficient = 0.81) at the basin outlet. Our findings show that sediment yields in the Yellow River Basin are more sensitive to precipitation rates than precipitation amounts. Halving rainfall intensity significantly reduces sediment discharge to the river, while halving rainfall amount reduces it by 60%. Doubling agricultural water use can reduce sediment discharge by 10%.

1. Introduction

Understanding the dynamics of water erosion and sediment transport is crucial across multiple disciplines, including agriculture (Montgomery, 2007; Syvitski et al., 2005), hydraulic and sedimentation engineering (Rijn, 1986; Vanoni, 2006), hydrology (Fagundes et al., 2021; Gao et al., 2013), ecology (Newbold et al., 2015; Oost et al., 2007), and geomorphology (Dietrich et al., 2003; Tucker & Hancock, 2010). On a global scale, these processes play a fundamental role in transferring carbon and nutrients from terrestrial pools to rivers and oceans, influencing biogeochemical cycles and ecosystem functioning (Lal, 2003; Ludwig & Probst, 1996; Tan et al., 2017). In fluvial systems, sediment load depends not only on the river's sediment transport capacity but also on sediment supply from the upstream sources (Einstein, 1964; Julien, 2010). The supply is influenced by climate, soil erodibility, topography, vegetation, and human influences (e.g., tillage and conservation practices) in the upper catchment (Lal, 2017), while transport capacity largely depends on flow characteristics, as well as channel

Supervision: Eric J. R. Parteli, Yaping Shao
Validation: Cong Jiang
Visualization: Cong Jiang
Writing – original draft: Cong Jiang
Writing – review & editing: Cong Jiang, Eric J. R. Parteli, Yaping Shao

geometry and roughness (Julien, 2010). Anthropogenic activities, including water diversion and dam construction, further alter sediment fluxes (Wang et al., 2016).

Numerous models—empirical, conceptual, and process-based—have been developed to simulate water erosion and sediment transport, differing in complexity, data demand, and applicability (de Vente et al., 2013; de Vente & Poesen, 2005; Hajigholizadeh et al., 2018; Harmon et al., 2001; Merritt et al., 2003). Empirical models, such as the Universal Soil Loss Equation (USLE) and its revised version (RUSLE), rely on statistical relationships and rainfall-runoff factors (e.g., EI30) to estimate sheet and rill erosion, but they do not explicitly address sediment transport and deposition (Renard et al., 2017; Wischmeier & Smith, 1978). Conceptual models, including the Soil and Water Assessment Tool model, integrate empirical formulas within a broader hydrological framework, aiming to balance simplicity with process details (Arnold & Fohrer, 2005; Neitsch et al., 2011). Meanwhile, process-based models (e.g., European Soil Erosion Model, Limburg Soil Erosion Model, Système Hydrologique Européen—Soil Erosion and Deposition, Water Erosion Prediction Project, Rangeland Hydrology and Erosion Model) explicitly represent sediment detachment, transport, and deposition but often require high-resolution data and significant computational resources, posing challenges for large-basin applications (Lukey et al., 1995; Morgan et al., 1998). A brief review of these models is presented in Text S1 in Supporting Information S1.

Despite significant advances in erosion modeling, large-scale predictions remain highly uncertain due to the complexity and interdependence of erosion and sediment dynamics, spatiotemporal variability in runoff and sediment transport, and limited observational data (Mao et al., 2010; Pelletier, 2012; Stewart et al., 2017; Tan et al., 2017; Van Rompaey et al., 2001; Vigiak et al., 2017). Accurately estimating sediment balance in large catchments is further complicated by the heterogeneity of model input data and parameters, which makes it difficult to scale models effectively across diverse spatial and temporal scales (de Vente & Poesen, 2005; Jakeman et al., 1999; Merritt et al., 2003; Morgan & Nearing, 2011). A key question is whether land surface and large-scale hydrological models, operating at resolutions of 1–30 km, can reliably capture sediment discharge in large watersheds (de Vente & Poesen, 2005; Morgan & Nearing, 2011).

Specifically, a major limitation of large-scale erosion models is the uncertainty in estimating the sediment transport capacity of overland flow, which varies with flow depth, slope, and roughness (Ali et al., 2013; Hessel & Jetten, 2007). On steep landscapes such as the Chinese Loess Plateau, transport equations with lower slope dependency (e.g., Govers, 1990) outperform other models, yet they often overestimate transport on steep slopes and underestimate it on gentle slopes (Hessel & Jetten, 2007). Rainfall-runoff erosivity, particularly the EI30 index, is a robust predictor of soil loss (Kinnell & Risse, 1998; Panagos et al., 2015; Yue et al., 2022), yet process-based models frequently neglect raindrop impact as a critical driver of sheet and rill erosion (Kinnell, 2005). Moreover, the inability to accurately simulate surface runoff spatially on the basin scale remains a major limitation of sediment yield models (Lane et al., 1997; Nearing, 2000). Studies suggest that runoff-driven models such as the Morgan model (Morgan et al., 1984) outperform rainfall-driven models (e.g., Pelletier and RUSLE models) (Pelletier, 2012; Renard et al., 2017) in capturing sediment dynamics (Tan et al., 2018).

Scaling issues, such as precipitation intensity decay and terrain coarsening, complicate regional erosion modeling (Mao et al., 2010; Yu et al., 1999). The lack of heterogeneity in land surface parameters and precipitation at large scales leads to underestimated runoff and inaccurate hydrological responses (Yu et al., 1999). Addressing these challenges requires incorporating subgrid-scale variability. Mao et al. (2010) improved soil erosion modeling by coupling Variable Infiltration Capacity model with Water Erosion Prediction Project–Hillslope Erosion model and using monofractal rescaling (Bowling et al., 2004) to restore fine-resolution slope details. Large-scale models must account for these scale effects to enhance accuracy.

Furthermore, gully erosion can dominate sediment supplies in large basins, but it is often underrepresented in models (de Vente & Poesen, 2005; Poesen et al., 2003). On the Chinese Loess Plateau, permanent gullies dominate the sediment supply, making accurate representation of gully erosion essential for realistic regional-scale simulations (Li et al., 2003; Wu & Cheng, 2005). However, modeling gully erosion remains challenging due to the limited representation of concentrated flow-driven and stochastic gravity erosion (Xu, 1999) and scarce data on gully morphology (De Geeter et al., 2023). While some insights could be gained from logistic probability models and 3D scanning (De Geeter et al., 2023; Li et al., 2017), a new approach to integrate gully erosion into regional-scale hydrological modeling is required.

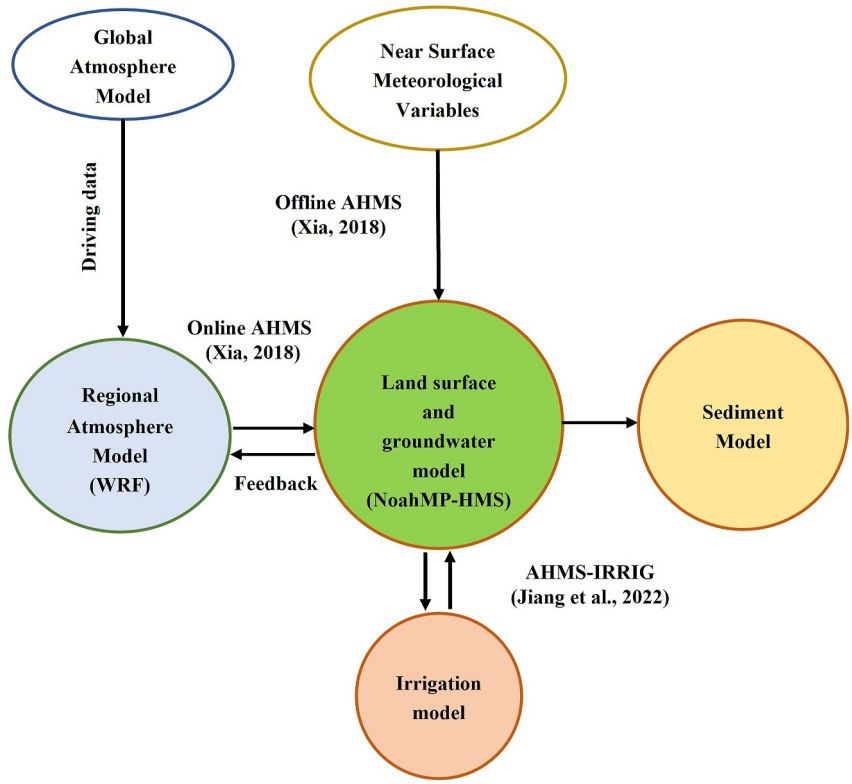

Figure 1. A simplified flowchart of the Atmospheric and Hydrological-Sediment Modeling System (AHMS-SED), integrating the Atmospheric and Hydrological Modeling System with a modified water erosion and sediment transport model (CASC2D-SED).

This study aims to develop an integrated soil erosion and sediment transport model—the Atmospheric and Hydrological-Sediment Modeling System (AHMS-SED)—designed for regional-scale applications. AHMS-SED incorporates gully erosion processes into the land surface and hydrological models, addressing a critical gap in large-scale sediment modeling. To overcome the limitations of previous models, AHMS-SED employs a detachment-transport coupling approach, integrating both rainfall-runoff erosivity (e.g., EI30) and runoff-based erosivity equations as multi-parameterization options. Importantly, AHMS-SED represents a fully coupled hydro-meteorological system, simulating the complete hydrological cycle from groundwater flow to atmospheric boundary layer interactions. It captures key processes such as runoff and sediment generation, flow and sediment routing, deposition, gully erosion, and river irrigation, ensuring a more comprehensive understanding of sediment dynamics across diverse landscapes and hydrological conditions.

This study addresses the following key scientific questions:

1. How can sediment detachment and transport capacity be effectively parameterized within a large-scale hydrological framework? Moreover, which erosivity predictors—rainfall, runoff, or overland flow—yield the most reliable results?
2. What scale effects, such as precipitation intensity decay and terrain coarsening, must be considered in large-scale erosion and sediment transport models?
3. How can gully erosion be effectively integrated into large-scale hydrological models to capture its role in regional sediment budgets?

2. Atmospheric and Hydrological-Sediment Modeling System (AHMS-SED)

2.1. Introduction to AHMS-SED

The AHMS-SED was developed by revising the water erosion and sediment transport model, CASC2D-SED (Rojas et al., 2003), and integrating it with the AHMS-IRRIG (Jiang et al., 2022). A schematic diagram of the

AHMS-SED is shown in Figure 1. Atmospheric and Hydrological Modeling System (AHMS) combines the regional atmosphere model Weather Research and Forecasting (WRF) model with the Hydrological Modeling System (HMS) (Xia, 2019; Yu et al., 2006) through the land surface model Noah-MP (Niu et al., 2011). AHMS can operate both online and offline. Online AHMS is coupled with WRF, while offline AHMS is driven by external near-surface meteorological data. The Noah land surface model with Multiple-Parameterizations (Noah-MP, version 1.6), as described by Niu et al. (2011), simulates the exchanges of heat, water, and momentum fluxes between the terrestrial land surface and the atmosphere.

The HMS was developed by Yu et al. (2006) for mesoscale hydrological simulation. It consists of a two-dimensional channel routing model (RT2D), a two-dimensional groundwater model (GW2D), and a groundwater channel interaction model. Surface runoff is simulated by considering the infiltration-excess runoff and the infiltration capacity equation (Jiang et al., 2022). The models use prognostic equations: the diffusive wave equation predicts overland and river water levels, the Boussinesq equation forecasts groundwater levels and Darcy's law estimates the interaction fluxes between rivers and groundwater. An irrigation module, referred to as AHMS-IRRIG (Jiang et al., 2022), has been integrated into AHMS to account for river and groundwater irrigation in arid and semi-arid river basins. Offline AHMS-IRRIG has been applied to the Yellow River Basin and shown to accurately simulate a broad range of hydrological processes—including runoff, streamflow, evapotranspiration, irrigation, and terrestrial water storage changes in the Yellow River Basin (Jiang et al., 2022). The timestep for the offline AHMS-SED is sub-daily or sub-hourly for the hydrological, sediment, and land surface components.

The objective of the new water-erosion and sediment module is to quantify the sediment discharge in the watershed, integrated into the AHMS framework. The surface runoff generation and sub-grid channel routing models are described in Section 2.2. The original CASCade 2-Dimensional SEDiment (CASC2D-SED) model is described in Section 2.3. Revisions to CASC2D-SED and the coupling with AHMS-SED are described in Section 2.4.

2.2. Surface Runoff and Sub-Grid Channel Routing Model

The rainfall-runoff model in AHMS employs infiltration capacity (I_{max}) (Largeron et al., 2018) to determine the proration between infiltration and surface runoff:

$$I_{max} = \beta K_{sat} \tag{1}$$

$$R_{ins} = \max(0, Q_{wat} - I_{max}) \tag{2}$$

$$I_{sfc} = Q_{wat} - R_{ins} \tag{3}$$

where β is an empirical parameter, calibrated based on the annual average runoff observed in the sub-basins, K_{sat} is the saturated hydraulic conductivity of surface soil, R_{ins} denotes the infiltration-excess runoff, Q_{wat} is the precipitation rate, and I_{sfc} is the infiltration rate.

The AHMS calculates overland and channel flow across large-scale domains using a subgrid channel routing model. The continuity equation is formulated by integrating mass continuity within individual cells and applying the Manning equation alongside the diffusive wave approximation to represent momentum transport between grids.

$$A\frac{\partial h_r}{\partial t} = \frac{\partial}{\partial x}\left(A_c \frac{1}{n} R_h^{2/3} \frac{\partial h_r}{\partial x}\left|\frac{\partial h_r}{\partial x}\right|^{-\frac{1}{2}}\right) + \frac{\partial}{\partial y}\left(A_c \frac{1}{n} R_h^{2/3} \frac{\partial h_r}{\partial y}\left|\frac{\partial h_r}{\partial y}\right|^{-\frac{1}{2}}\right) + R_{sf} - q_{gw} - q_{irr\_sf} \tag{4}$$

where A represents the riverbed area of water in the river or lake (m^2), h_r is the elevation of the water surface in the river or lake (m), A_c denotes the cross-sectional area of water in the river or lake at cell boundaries (m^2), n stands for Manning's roughness coefficient (s $m^{-1/3}$), and R_h is the hydraulic radius (m), R_{sf} is the surface runoff (m^3 s^{-1}), which comprises the infiltration-excess runoff (R_{ins}) and the saturation-excess runoff (R_{sat}), q_{gw} is the water flux interactions between groundwater and channel (m^3 s^{-1}), q_{irr_sf} refers to the river irrigation (m^3 s^{-1}). Furthermore, for every grid cell in the square lattice constituting the simulation domain, Equation 4 is solved by considering both nearest neighboring cells in x and y directions, as well as in the diagonals (omitted from

Equation 4 for clarity). Additionally, the term $\frac{\partial h_r}{\partial x}\left|\frac{\partial h_r}{\partial x}\right|^{-\frac{1}{2}}$ in Equation 4 is a modification of $\left(\frac{\partial h_r}{\partial x}\right)^{\frac{1}{2}}$, designed to handle situations where $\frac{\partial h_r}{\partial x}$ is negative.

The Manning equation is used to estimate the average velocity V (m s^{-1}) of the river flow cross-section,

$$V = n^{-1} R_h^{2/3} S_f^{1/2} \tag{5}$$

where S_f is the friction slope (−), representing the energy loss due to friction. In this study, we apply the diffusive wave approximation by neglecting the local and convective acceleration terms, assuming the flow is dominated by pressure, gravitational and frictional forces. Thus, S_f is approximated as the slope of the elevation of the water surface, as shown below.

$$S_f = S_w = \frac{\partial h_r}{\partial x} = S_0 - \frac{\partial h}{\partial x} \tag{6}$$

where S_0 is the bed slope (−), S_w is the water surface slope (−), and h is the depth of water (m).

The hydraulic geometric shape of the channel is modeled using power-law functions based on the bank full discharge (Q_{BF}), as per Leopold and Maddock (1953).

$$\begin{cases} w = aQ_{BF}^{b} \\ d = cQ_{BF}^{f} \end{cases} \tag{7}$$

The coefficients a and c, along with exponents b and f, are determined from observations. Common values are $b = 0.5$ and $f = 0.3$, with assumed values of $a = 5.0$ and $c = 0.6$ based on river width measurements and shallow cross-sections in the Yellow River Basin. The minimum values for channel width and depth are set at 10 and 2 m, respectively, to meet the model requirements. Thus, the river width and depth are defined as follows

$$\begin{cases} w = \max\left(5.0 \cdot Q_{BF}^{0.5}, 10\right) \\ d = \max\left(0.6 \cdot Q_{BF}^{0.3}, 2\right) \end{cases} \tag{8}$$

2.3. Original CASCade 2-Dimensional SEDiment (CASC2D-SED) Model

The original iteration of the CASCade 2-Dimensional SEDiment (CASC2D-SED) model was founded upon a two-dimensional overland flow routing algorithm developed by Julien et al. (1995) at Colorado State University. Johnson (1997) incorporated the upland erosion and channel sediment transport module to CASC2D, called CASC2D-SED, and built upon earlier work of Kilinc (1972) and Kilinc and Richardson (1973). Rojas (2002) further enhanced the sediment transport algorithms in CASC2D-SED by improving the simulation of transition between supply-limited and capacity-limited transport, allowing for the advection of suspended material even with negligible transport capacity and enhancing sedimentation simulation in backwater areas. For a description of the original CASC2D-SED, refer to Rojas (2002).

The model has the following characteristics:

1. The transport capacity of overland flow (caused by the sheet and rill erosion) is estimated by the modified Kilinc-Richardson equation which combines the Kilinc-Richardson equation and soil erodibility (K factor), vegetation (C factor) and land use practice (P factor) from USLE.
2. The transport capacity of channel flow is estimated using the Engelund and Hansen equation (1967) based on hydraulic parameters (hydraulic radius, flow velocity, and friction slope) and particle characteristics (specific gravity and particle diameter).
3. Once suspended, the sediment is transported through advection even under transport capacity-limited conditions.

4. The particle sizes are divided into three size classes: sand, slit and clay (see Table S5 in Supporting Information S1). The median of the corresponding particle size distribution (d_{50}) is used for each class to characterize the particle sizes associated with the sand, silt and clay classes. The settling time of particles is then calculated according to the settling velocity (refer to Text S5 in Supporting Information S1) and water depth.

2.3.1. Sediment Transport Approximation

Once eroded from the soil, a soil particle is entrained into the water flow and transported downstream in the watershed. At any downstream cross-section, sediment flux is mainly controlled by sediment availability and stream transport capacity. The water flow easily carries the finer material (clay), so its transport is limited mainly by the sediment supply in the watershed. By contrast, the coarse material (sand) is associated with higher resistance to flow. Transport of this coarse material is, therefore, limited mainly by the transport capacity of the flow. Furthermore, fine material is transported primarily in suspension as wash load, while the transport of the coarse material occurs mainly as (near-surface) bed load. Therefore, the total sediment load consists of the wash load of fine particles and the bed load of coarse grains. The processes of upland soil erosion and upland and channel sediment transport can be summarized through steps 1–4 (see also Figure S2 in Supporting Information S1).

Step 1: The transport capacity of the water flow is calculated using the modified Kilinc and Richardson's equation (1973) for overland flow and Engelund and Hansen's equation (1967) for channel flow.
Step 2: The transport capacity of the water flow is used to estimate the transport rate of the suspended sediment for the various particle size fractions considered.
Step 3: Deposited sediment is entrained into suspension transport based on the excess transport capacity, that is, the total transport capacity minus the amount of suspended sediment.
Step 4: If the total sediment transport capacity exceeds the amount of suspended and deposited sediment, then bed soil erosion in the upland occurs. The percentage of soil eroded is proportional to the percentage of the corresponding size fraction of the parent material. However, channel erosion is not considered.

2.3.2. Upland Erosion and Sediment Transport

Kilinc (1972) and Kilinc and Richardson (1973) studied sheet and rill erosion using flume experiments and derived an equation Kilinc and Richardson's equation (KR) for predicting sediment discharge in uniform flow over the bare sandy soil. They found that unit sediment discharge, denoted as q_s (tons m^{-1} s^{-1}), increases with the square of water discharge and with the 5/3 power of the slope. Furthermore, Julien (2010) modified the KR equation to account for non-uniform flows by considering soil erodibility index, vegetation cover or cropping management factor and conservation practice factors, which are parameters encoded in USLE. The equation for $q_{s,}$ the unit sediment discharge (ton m^{-1} s^{-1}), reads

$$q_s = 23210 \cdot {S_0}^{5/3} \cdot q^2 \cdot K \cdot C \cdot P \tag{9}$$

where S_0 is the slope gradient in per cent, q is the unit water discharge, K is the soil erodibility index in the USLE equation, C is the vegetation cover or called crop factor in USLE equation (−), and P is the practice factor in USLE equation (−).

2.3.3. Sediment Transport Capacity of River

The stream transport capacity is calculated using the Engelund and Hansen equation. The equation of Engelund and Hansen (1967) employs Bagnold's stream power model and the similarity principle to estimate the sediment concentration by weight, which is called transport capacity in the river. The equation reads,

$$C_{w,i} = 0.05 \cdot \left(\frac{G_s}{G_s - 1}\right) \frac{V \cdot S_f}{\sqrt{(G_s - 1) \cdot g \cdot d_{s,i}}} \sqrt{\frac{R_h \cdot S_f}{(G_s - 1) \cdot d_{s,i}}} \tag{10}$$

where $C_{w,i}$ is the sediment concentration of flow by weight for the size fraction i (−), G_s is the sediment specific gravity (−), V is the averaged velocity of the channel (m s^{-1}), R_h is the hydraulic radius, as used in Equation 4, S_f is

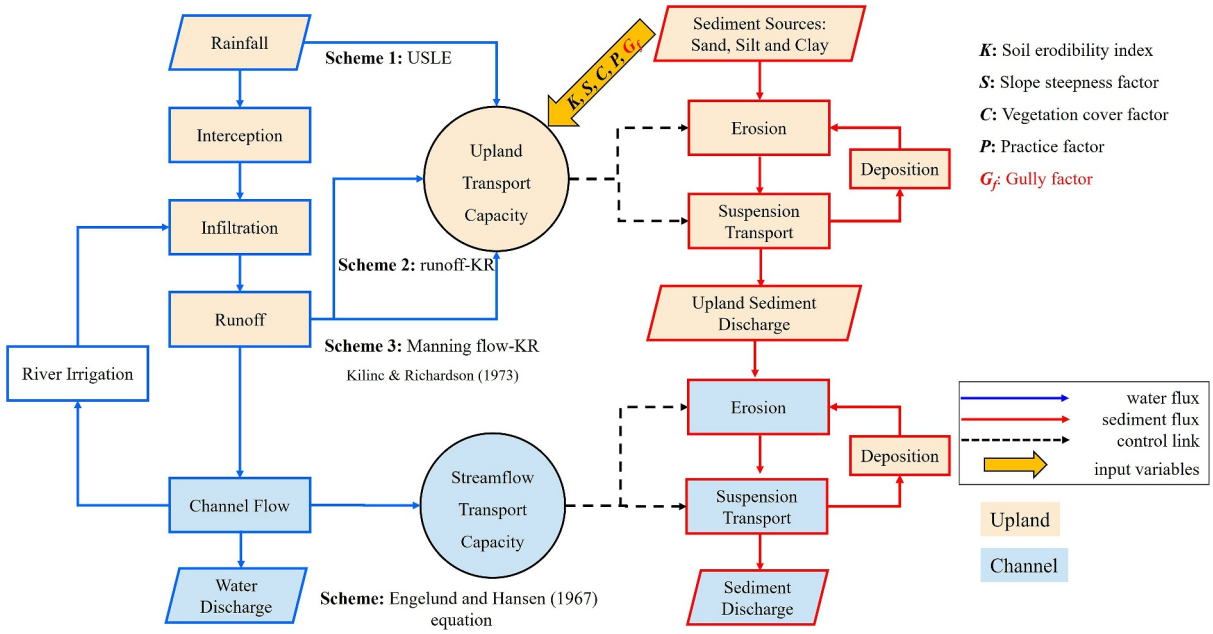

Figure 2. A simplified flowchart illustrating the processes integrated into the model, combining the hydrological processes within AHMS-IRRIG with water erosion and sediment transport processes in CASC2D-SED.

the friction slope of the channel (−), g is the gravitational acceleration (m s^{-2}), $d_{s,i}$ is the size diameter (m) of fraction i.

2.4. Modifications to CASC2D-SED and Coupling With AHMS

The CASC2D-SED module was revised to align with the large-scale sub-grid flow routing model in AHMS. Modifications include implementing multiple sediment transport equations for overland flow, addressing scaling issues in soil erosion prediction, and incorporating gully erosion representation. Figure 2 illustrates the integration of large-scale hydrological processes with water erosion and sediment transport within the AHMS-IRRIG framework.

Originally developed for small-scale hydrological models, CASC2D-SED differentiates between overland and channel grids, applying upland erosion only to overland grids. For larger-scale applications in AHMS-SED, the upland erosion component has been adapted to operate for each grid. Based on the observed river network, streamflow transport capacity is only calculated for the main river, where the bank height exceeds a threshold of 2 m.

Using hydrological variables from AHMS, three distinct methods for calculating upland transport capacity have been developed:

1. Rainfall intensity combined with the USLE.
2. Surface runoff rate applied to the Kilinc and Richardson Equation.
3. Surface runoff rate integrated with both the Manning Equation and the Kilinc and Richardson equations.

Additionally, the upland sediment transport capacity model has been revised to incorporate the USLE and Kilinc and Richardson equations, with enhancements to account for gully erosion through the integration of a gully factor.

2.4.1. Development of a Unified Upland Sediment Transport Capacity Equation

In this study, we aim to develop a unified large-scale (coarse resolution, in kilometers) water erosion and sediment transport module by incorporating only basic independent variables, which are available in a mesoscale land surface and hydrological model within the framework of AHMS-SED. However, the derivation of a general relationship between large-scale, overland water flow-induced soil erosion and the relevant environmental factors

poses a challenging task due to the complex and interdependent nature of erosion and sediment dynamics. The process is governed by the intricate interplay of climate (rainfall and runoff), soil properties (erodibility), topography (slope), ground cover (vegetation and rock), and human activities (tillage and conservation practices), yet their interactions are not well understood. By following the dimensional analysis approach of Julien & Simons (1985), the upland sediment discharge caused by sheet erosion in overland flow can be modeled as a function of basic independent variables using the following scaling relation:

$$\frac{q_s}{\rho\nu} = e_1 {S_0}^{e_2} \left(\frac{q}{\nu}\right)^{e_3} \left(\frac{r_i X_r}{\nu}\right)^{e_4} \left(1 - \frac{\tau_{cr}}{\tau_0}\right)^{e_5} \tag{11}$$

where q_s is the rate of mass transport per unit width, S_0 is the bed surface slope, q is the unit discharge, r_i is the rainfall intensity, X_r is the length of runoff, ρ is the mass density of the fluid, υ is the kinematic viscosity of the fluid, τ_{cr} and τ_0 are critical and bed surface shear stresses, respectively. The coefficients e_1, e_2, e_3, e_4, and e_5 can be determined through laboratory or field investigations. Various sediment transport capacity equations for overland flow can be unified within this general relationship using laboratory data, with the exponents provided in Table S1 in Supporting Information S1.

However, overland flow includes not only the diffuse sheet flow (laminar or mixed laminar flow) but also concentrated flow (turbulent flow) in rill or gullies (Ward & Robinson, 1975). Specifically, gully erosion represents a more advanced and severe form of erosion than sheet and rill erosion, which USLE/RUSLE typically predicts. These models do not account for concentrated flow processes that lead to gully formation nor predict gully erosion rates or specific locations where gullies might form. Introducing a gully erosion factor could address this gap by representing these concentrated flow processes and helping to pinpoint potential gully formation sites. Thus, the above dimensional analysis is further extended, along with physical model assessments, by considering the confinement of flow geometry in the gully, as detailed in Text S2 in Supporting Information S1.

Dimensional analysis requires:

$$\frac{q_s}{\rho\nu} = e_1 {S_0}^{e_2} \left(\frac{q}{\nu}\right)^{e_3} \left(\frac{r_i X_r}{\nu}\right)^{e_4} \left(1 - \frac{\tau_{cr}}{\tau_0}\right)^{e_5} {G_{af}}^{e_6} \tag{12}$$

where G_{af} represents the gully area fraction, which is the gully area divided by the grid cell area (see Eq. S2). We assume that the gully area factor (G_f), which represents the enhancement of erosion rate caused by concentrated flow in the gully, is given by $G_f = {G_{af}}^{e_6}$.

Following Julien & Simons (1985), this equation can be further simplified under two assumptions: (a) When τ_{cr} remains small compared with τ_0, the last term can be neglected. (b) For one-dimensional overland flow, on the impervious surface, the unit flow discharge is equal to the rainfall rate multiplied by the runoff length, that is, $q = r_i X_r$. Thus, the second and third terms are alternative and dependent.

We note that this model can be separated into the contributions from the rainfall and runoff variables (Table S4 in Supporting Information S1), which are associated with the typical USLE and KR equations, respectively:

$$\text{Rainfall type: } \frac{q_s}{\rho\nu} = e_1 {S_0}^{e_2} \left(\frac{r_i X_r}{\nu}\right)^{e_4} {G_{af}}^{e_6} \tag{13}$$

$$\text{Runoff type: } \frac{q_s}{\rho\nu} = e_1 {S_0}^{e_2} \left(\frac{q}{\nu}\right)^{e_3} {G_{af}}^{e_6} \tag{14}$$

Therefore, although the USLE and the KR equation were originally developed for estimating sheet and rill erosion, the rainfall-runoff erosivity from the USLE and the runoff erosivity from the KR equation can also be combined with a gully factor to predict upland erosion, including in areas affected by gullies.

2.4.2. Rainfall-Runoff Erosivity (EI30) Based Upland Sediment Transport Capacity

The USLE, as mentioned earlier, has been developed to predict long-term soil erosion based on different environmental factors. To calculate the sediment discharge in the upland areas of the Yellow River Basin, we extend

the USLE to incorporate additional parameters associated with the sediment supply from gully erosion. Specifically, the equation for $q_{s,}$ the unit sediment discharge (ton m^{-1} s^{-1}), reads

$$q_s = e_1 \cdot E \cdot I_{30}\, S \cdot K \cdot C \cdot P \cdot G_f \tag{15}$$

where q_s is the sediment discharge based on the USLE with the modification introduced in the present study (ton ha^{-1} yr^{-1}), and e_1 is a dimensionless free parameter, which needs to be calibrated with the help of sediment discharge data, K is the soil erodibility index (ton ha h ha^{-1} MJ^{-1} mm^{-1}), S is the slope steepness factor (−), C is the vegetation cover or called crop factor (−), and P is the practice factor (−), G_f is the gully area factor (−), E is the rainfall kinetic energy for the time interval Δt (MJ ha^{-1}) (see Text S4 in Supporting Information S1), and I_{30} is the maximum 30 min rainfall intensity (mm h^{-1}) during a storm. In the USLE, EI30 values are calculated using breakpoint rainfall intensity data derived from continuous recordings on rain gauge charts. However, in the land surface model, only fixed-interval (such as hourly) rainfall data is available. Thus, in this study, the 30-min rainfall erosivity index (EI30) was derived from sub-daily rainfall data (e.g., 3-hourly CMFD; see Section 3.2.1) by multiplying a fixed conversion ratio, following Yin et al. (2007) and a regression fit (Figure S3 in Supporting Information S1) for estimating rainfall erosivity from fixed-interval data in China.

2.4.3. Runoff-Based Upland Sediment Transport Capacity

Similarly, the KR equation, the modification of Julien (2010), is further improved to incorporate concentrated flow in the gullies. As discussed in the previous section, this extension is essential for the accurate modeling of sediment transport capacity at the regional scale. Specifically, the sediment discharge q_s is assumed to be proportional to the gully factor G_f by taking into account concentrated flow and additional parameters related to sediment supply due to gully erosion. The equation for $q_{s,}$ the unit sediment discharge (ton m^{-1} s^{-1}), reads

$$q_s = e_1 \cdot {S_0}^{5/3} \cdot q^2 \cdot K \cdot C \cdot P \cdot G_f \tag{16}$$

where e_1 is a dimensionless free parameter, which needs to be calibrated with the help of sediment discharge data; S_0 is the soil slope (m m^{-1}), G_f is the gully area factor (−), and q is the unit flow discharge (m^2 s^{-1}).

In land surface and flow routing models, "surface runoff rate" refers to the vertical accumulation of water on land, while "flow velocity" describes its horizontal movement across the surface or through rivers. These distinctions are essential for understanding runoff generation and water movement dynamics. Additionally, according to the principle of mass conservation, for one-dimensional overland flow, the unit flow discharge is equal to the runoff rate multiplied by the runoff length on the slope. In this study, the overland flow is incorporated here by computing the unit discharge q of overland flow both from the surface runoff rate (R_s) and using Manning's equation. In the Manning equation, the slope of the energy line is equal to the slope of the soil surface (kinematic wave approximation). It is given by

$$q = \begin{cases} R_{sf} \cdot dx \\ \dfrac{1}{n} \cdot R^{\frac{5}{3}} \cdot {S_0}^{\frac{1}{2}} \end{cases} \tag{17}$$

where R_{sf} is the surface runoff rate (m s^{-1}), dx is the width of grid cells applied in the simulations (m), n is the Manning roughness coefficient, which is selected according to the type of ground cover, and R is the hydraulic depth (m).

2.4.4. Incorporation of Erosion Factors: *K, S, C, P* and G_f

In the original USLE, the soil erodibility factor (K) encodes information about the inherent resistance of sediment on the soil to water erosion, which is related to soil texture, organic matter and permeability. Many studies have found that soil erodibility is mainly associated with clay content (CL). Zhang et al. (2004) developed and validated, thus, the following soil erodibility equation related to CL using experimental field data from the Chinese Loess Plateau.

$$K = 0.031 - 0.0013 \cdot \mathrm{CL} \tag{18}$$

where CL is the clay content in percentage (%).

The length and slope factors (L and S, respectively) represent the geomorphological controls in the original USLE. Since it is difficult to represent the slope length factor L in a catchment-scale domain, Pelletier (2012) suggests using S as the only geomorphological control parameter and employing a model that is not based on L. We follow Pelletier (2012) and use the following equation for S.

$$S = 20 \cdot {S_0}^{5/4} \tag{19}$$

The crop factor is calculated based on the vegetation greenness and cropland fraction F_{veg} and F_{crop}, respectively, and it also accounts for the tillage method factor. To represent and quantify soil conservation practices on a large scale, we assume a practice factor P value of 1.0. Summarizing,

$$F_{\mathrm{veg}} = 1 - e^{-0.52 \cdot LAI} \tag{20}$$

$$C = f_{\mathrm{no-till}} \cdot (1 - F_{\mathrm{veg}}) + f_{\mathrm{till}} \cdot F_{\mathrm{veg}} \cdot F_{\mathrm{crop}} \tag{21}$$

where F_{crop} is the cropland fraction obtained from 500 m MODIS-based irrigation fraction (Ozdogan & Gutman, 2008). In the Yellow River basin, we have noted that irrigated cropland is more affected by tillage erosion, while rainfed areas are less impacted. Moreover, leaf area index (LAI) is the obtained from lookup tables on land use types and the calendar month. The adoption of table-based LAI, which is the standardized default option in the Dynamic Vegetation parameterization of Noah MP-LSM as outlined by He et al. (2023), has been validated and proven effective in a range of studies (Chen et al., 2016; Cuntz et al., 2016). f_{till} is the tillage method factor, which accounts for agricultural soil erosion due to plowing and tillage. For the cropland, we assumed to $f_{\mathrm{till}} = 1.0$. Furthermore, $f_{\mathrm{no\text{-}till}}$ represents the no-tillage method factor for nature land, which is typically less than 1.0. Wilkinson and McElroy (2007) suggested that soil erosion on cultivated land is four times greater than on natural land at a catchment-scale. In contrast, Maetens et al. (2012) reported that cropland experiences up to 10 times more erosion than natural land, based on a comprehensive analysis of measured plot studies in Europe. Therefore, we initially set the default value of $f_{\mathrm{no\text{-}till}}$ to 0.25. This parameter is also set to 0.1 in our sensitivity analysis to evaluate its influence on sediment discharge predictions.

In Section 2.4.1, we introduce and integrate a "gully factor" into the calculations for upland sediment discharge to account for the enhanced erosion attributed to concentrated flow in gully areas. The gully erosion factor is computed using the exponential equation here based on the gully area index. The gully area index is validated by comparing it to a boundary map of sediment-rich areas in the middle reaches of the Yellow River Basin, as detailed in Section 3.3.1. Additionally, the gully factor is further validated by comparing upland sediment transport capacity and sediment discharge at the basin outlet with and without the gully factor, as discussed in Section 4.2.

Specifically, a novel gully area index (G_a) to predict the permanent gully area fraction (gully areas/grid cell areas) on regional scales is proposed. We assume that the permanent gully area fraction describing the ground fragmentation can be estimated from the rate with which the slope decreases as the resolution of Digital Elevation Model (DEM) decreases. Here, the gully area index G_a is defined as the quotient ratio of $S_{30\ \mathrm{m}}$ and $S_{20\ \mathrm{km}}$, that is, the average slopes derived from the 30 m high-resolution DEM and the average slopes derived from the 20 km resolution DEM, respectively.

$$G_a = \frac{S_{30\ \mathrm{m}}}{S_{20\ \mathrm{km}}} \tag{22}$$

$$G_f = \exp(\alpha \cdot (G_a - 1)) \tag{23}$$

where $G_a \geq 1.0$ and α is an empirical dimensionless parameter tested through sensitivity analysis to calibrate and evaluate its influence on sediment discharge predictions at the basin outlet. The definition of slope and the interpolation method using raster data is detailed in Text S3 in Supporting Information S1.

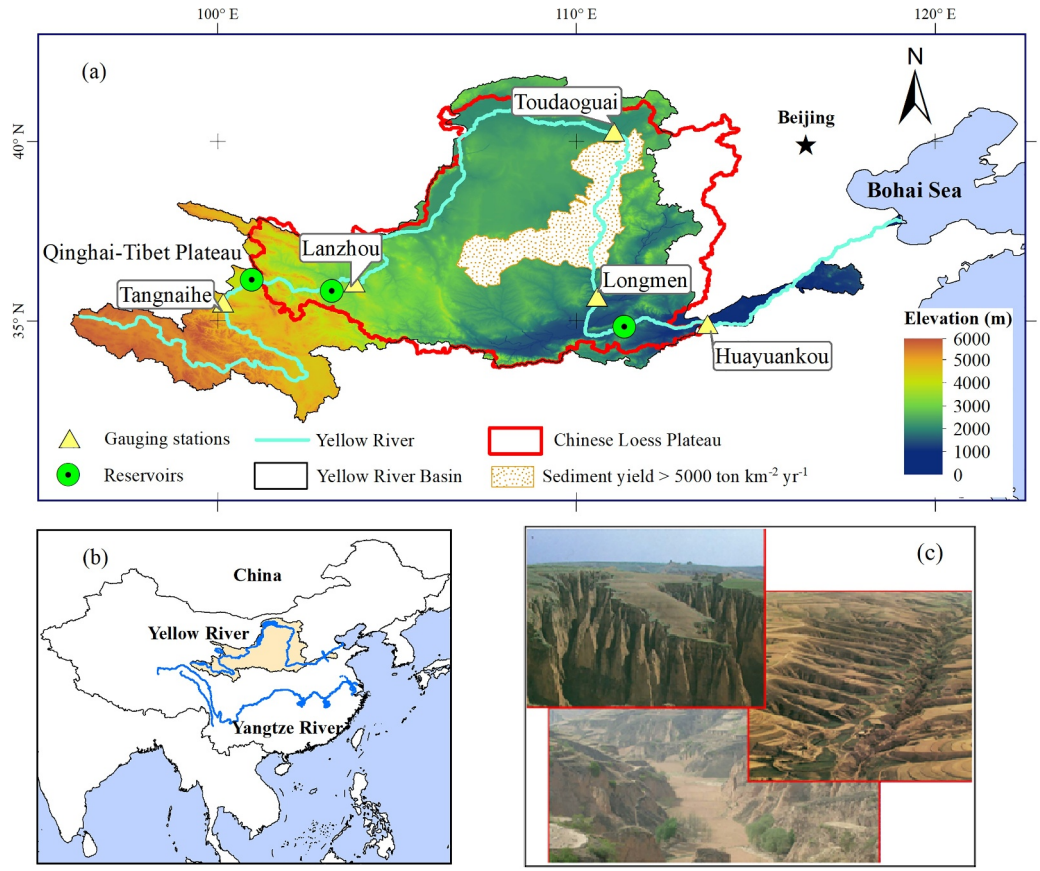

Figure 3. (a) Topography of the Yellow River Basin and the locations of the five main hydrological stations: Tangnaihai, Lanzhou, Toudaoguai, Longmen (LM) and Huayuankou. The dotted area, separating the stations of LM at the south and Toudaoguao at the north, corresponds to an area of permanent gully activity and very high-intensity water erosion. The sediment yield modulus within the time span from 1999 to 2019 exceeded 5,000 ton km^{-2} yr^{-1} in this area (http://www.ncdc.ac.cn). The major reservoirs indicated in the figure, from upstream to downstream, are Longyangxia, Liujiaxia, and Sanmenxia. (b) Regional location map; (c) A typical landscape of permanent gullies in the Loess Plateau.

3. Application to the Yellow River Basin

3.1. Study Area: Yellow River Basin

Notably, the world's most severe soil erosion occurs on the arid and semi-arid Chinese Loess Plateau. Figure 3 highlights the Loess Plateau, located in the middle reaches of the Yellow River, spanning 640,000 km^2 in northwest China. This region is characterized by an extensive loess cover and high erosion rates, averaging approximately 1.6 Gt yr^{-1} from 1950 to 1980 (Qian & Dai, 1980). Over 60% of the Loess Plateau experiences severe soil erosion, with an average soil loss of 2,000–2,500 ton km^{-2} yr^{-1} and about 0.01–2 cm of topsoil eroded annually (Shi & Shao, 2000). This world's highest soil erosion rate results from several factors, including high soil erodibility, sparse vegetation, large permanent gullies, intense and concentrated rainfall, and extensive long-term human activity (Hessel et al., 2003; Zheng & Wang, 2014).

The Yellow River is the second-longest river in China (5,464 km), and the Yellow River Basin (795,000 km^2) is the largest in northern China. The Yellow River flows across the Qinghai-Tibet Plateau, Inner Mongolia Plateau, Chinese Loess Plateau, and Huanghuaihai Plain. The annual mean air temperature in the Yellow River Basin ranges from −4° to 2°, and the annual mean precipitation is approximately 450 mm, which is unevenly distributed (Yellow River Water Bulletin). Additionally, the basin is characterized by a plateau and temperate climate and is strongly affected by the East Asian monsoon.

The mean annual runoff in Sub-basin 3, illustrated in Figure S4 in Supporting Information S1, is negative, attributed to irrigation water use in this region. Thus, irrigation water is a crucial component of the water balance, especially in the semi-arid areas of the Yellow River Basin. Additionally, the sediment discharge of the Yellow River increases significantly through the Loess Plateau. Figure S4 in Supporting Information S1 also shows that while 80% of the water yield comes from the upstream area of Toudaogai, this area supplies only 10% of the sediment load to the Yellow River. In contrast, nearly 90% of the sediment load originates from the midstream area (Toudaoguai (TDG)—Huayuankou (HYK)), characterized by the wind-deposited Loess Plateau. It is well-known that water and sediment yields are distinctly separated in the Yellow River Basin (Hassan et al., 2008). Furthermore, over the past 60 years, the sediment load of the Yellow River has decreased by approximately 90% (Yu et al., 2013) due to the reductions in water discharge and sediment concentration. These changes can be attributed to regional climatic variations and human interventions such as soil conservation on the Loess Plateau, increased water consumption, and several dams along the Yellow River (Wang et al., 2016; Yu et al., 2013).

3.2. Data and Preprocessing

3.2.1. Near Surface Meteorological Data

The high spatial-temporal resolution gridded China Meteorological Forcing Data set (CMFD) (Chen et al., 2015; He et al., 2020; Yang et al., 2015) is adopted as the near-surface meteorological input data set driving the land surface model. The associated variables include precipitation, near-surface air temperature, near-surface specific humidity, surface pressure, near-surface wind, surface downwelling shortwave and longwave radiation. Compared to various other gridded rain gauge-corrected precipitation data sets, CMFD has been validated as the most accurate precipitation product for the Yellow River Basin (Jiang et al., 2024).

3.2.2. Geo-Static Data

The DEM, including the information about hydrological systems in the study area, is used as the input variable for the flow and sediment routing model. Specifically, the high-resolution geographic digital elevation data set Multi-Error-Removed Improved-Terrain DEM with a 3-s resolution (Yamazaki et al., 2019a, 2019b) is used and upscaled to the model resolution (see Figure 4a) by using an HMS preprocessing program (Yu et al., 2006). The slope is calculated based on 30 m resolution DEM SRTM (Farr et al., 2007; JPL, 2013) and then aggregated to 20 km resolution (see Figure 4b) using the grid-cell average interpolator from the WRF Preprocessing System (WPS).

The study utilizes the United States Department of Agriculture 16-class soil classification system (Davis & Bennett, 1927; Soil Survey Division Staff, 1993) for categorizing soils. The State Soil Geographic Database Food and Agriculture Organization (STATSGO) and the Food and Agriculture Organization (FAO, 1991) soil data set provides the soil type map. Furthermore, soil type map and United States Geological Survey 24-category vegetation (land use) data sets are aggregated from 5 arc min resolution to model grid in the Yellow River Basin using the WPS, as shown in Figures 4c and 4d.

Additionally, the CL is obtained from a 30 arc-seconds resolution soil particle-size distribution data set, developed for regional land and climate modeling (Shangguan et al., 2012a, 2012b), and is used to calculate the soil erodibility factor. Furthermore, a basic boundary map of rich sediment areas (see Figure 4f) in the middle reaches of the Yellow River Basin (Yellow River Basin Monitoring Center, 2020)—defined as the area with a sediment transport modulus greater than 5,000 t km^{-2} a^{-1} and a widespread presence of permanent gullies—is used to validate the gully index.

3.2.3. Observed Hydrological and Sediment Data

To calibrate and validate the model predictions for the water and sediment discharge, we employ the daily averaged measured water discharge (m^3 s^{-1}) and suspended sediment concentration (kg m^{-3}) for the period 1979–1987 from the National Earth System Science Data Center, China, including the five major stations along Yellow River, namely Tangnaihai (TNH) (a), Lanzhou (LZ) (b), TDG (c), Longmen (LM) (d) and HYK (e). The method for measuring suspended sediment concentration at river locations involves collecting instantaneous bucket samples to determine the river water volume-averaged concentration.

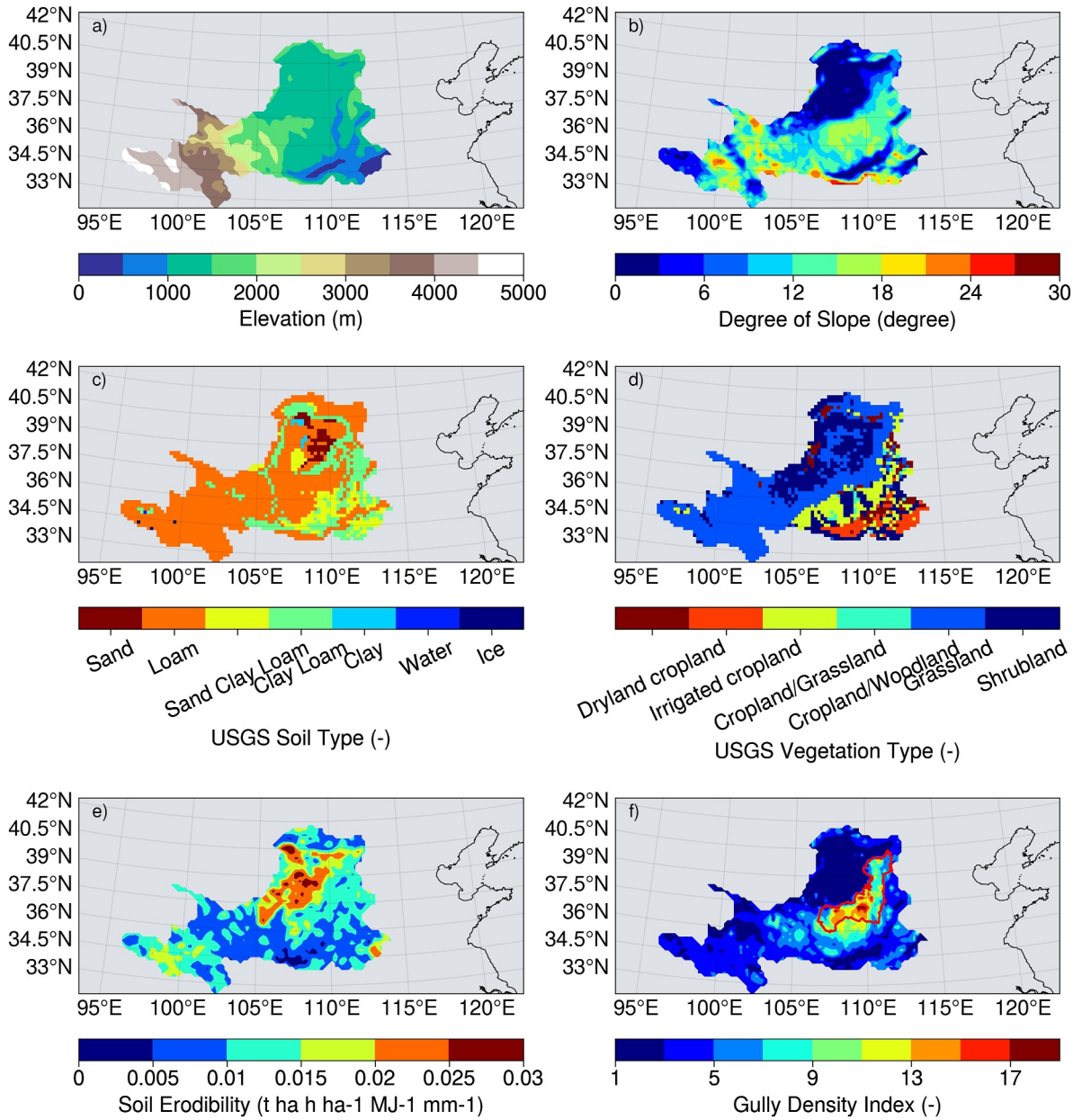

Figure 4. The input geo-static data include elevation (a), slope (b), soil type (c), vegetation type (d), soil erodibility (e) and gully density (f) index for the Yellow River Basin. In subplot (f), the red line represents sediment source hotspots in the middle reaches of the Yellow River, the Loess Plateau of China.

3.3. Model Configuration and Experimental Setup

3.3.1. Model Configuration

The spatial and temporal resolutions of the offline AHMS-SED are 20 km and 60 min, respectively. Here, we focus on streamflow simulations around the 1980s, that is, the early years preceding the construction of the dams, since our model currently does not consider the role of dams and reservoirs in regulating river flow and suspended sediment. Furthermore, a 20-year climatological spin-up, using constant geostatic data and cyclic forcing from 1979 to 1989, is performed to reach equilibrium conditions within the model, particularly for the groundwater table, before conducting the experiments described in this paper. The geo-static variables are re-gridded into the modeled domain in the Yellow River Basin. Figure 4a shows that the western part of the Yellow River Basin (Qinghai-Tibet Plateau) has high elevations, while the eastern regions are lower. Figure 4b illustrates that the

southern and western slopes of the Yellow River Basin are steep, whereas the northern region is notably flat. Figure 4c indicates that loam is the dominant soil type in the Yellow River Basin. Figures 4d and 4e show that grassland and shrubland are prevalent vegetation types and soil erodibility is high in the flat northern areas of the Loess Plateau. The distribution of the gully area index, as shown in Figure 4f, is closely related to the areas rich in sediment and permanent gullies. The calibrated parameters are selected from the land surface model, the flow routing model, the irrigation module, and the water erosion and sediment transport model, as detailed below.

3.3.1.1. Hydrological Model

The regional hydrological model of the Yellow River Basin, which forms the basis for the water erosion and sediment transport model setup in this paper, was developed in a previous study by Jiang et al. (2022). This previous study includes the sensitivity analysis of the model parameters referred to in the present manuscript, specifically for the parameters include the soil saturated hydraulic conductivity, saturated hydraulic conductivity of riverbed, riverbed fraction and Manning's roughness coefficients, irrigation triggered soil water availability and triggered leaf area (Jiang et al., 2022). Jiang et al. (2022) calibrated and validated the regional hydrological model of the Yellow River Basin with consideration of irrigation by comparing observed and predicted water discharge, evapotranspiration and terrestrial water storage change using in-situ, satellite and assimilated data. A summary of the physical and control parameterization schemes used in the land surface model (Noah-MP) is listed in Table S2 in Supporting Information S1. For a comprehensive understanding of the hydrological parameterization used in this model, please refer to Jiang et al. (2022).

3.3.1.2. Water Erosion and Sediment Transport Model

Three parameters within the erosion and sediment transport module of AHMS-SED are selected for the parameter sensitivity analysis. These three parameters are the empirical parameter in the gully factor equation (α), the scaling parameter in the overland flow transport capacity equation (e_1) and the no-tillage parameter in the crop factor equation ($f_{\text{no-till}}$).

We calibrate the offline AHMS-SED against the observed average sediment yields at the HYK station from 1 January 1979 to 31 December 1983. Therefore, the offline AHMS-SED is validated by comparing the observations and predictions of monthly sediment fluxes at five hydrological stations from 1 January 1984 to 31 December 1987.

3.3.2. Experimental Design

We designed 21 numerical experiments to calibrate and validate the AHMS-SED model. Each experiment includes a calibration period (1979–1983) and a validation period (1984–1987), which are crucial for ensuring the robustness of the experimental results. As shown in Table 1, the experiments are organized into three distinct groups: Ensembles I, II, and III. Each ensemble uses different sediment transport equations for upland areas based on rainfall, runoff, and overland flow as erosivity predictors.

The calibration process for each experiment involves adjusting three main parameters: the free parameter (e_1), the empirical parameter in the gully factor equation (α), and the no-tillage factor ($f_{\text{no-till}}$). To simplify the calibration process, we select fixed sets of the gully factor (0, 0.2, 0.3, 0.4) and the no-tillage factor (0.1 and 0.25). These fixed sets have been selected based on results from pre-calibration tests, by comparing the observed sediment discharge with model prediction results for different values of the gully factor, while the values chosen for the no-tillage factor fixed sets fall within the range reported in previous work (Maetens et al., 2012; Wilkinson & McElroy, 2007). Using these fixed sets of the gully factor and the no-tillage factor, the free parameter (e_1) is then calibrated for each experimental setup, whereupon a parameter sensitivity test is performed to elucidate the significance of gully and crop factors on the model predictions. All experiments use the same relevant sediment modules, including the sediment routing module and the equations for sediment transport capacity and deposition velocity, to ensure consistency across the experiments.

While the model operates at an hourly time step and daily data are available, we chose to perform calibration and validation on a monthly basis. This decision is driven by the complexities of the Yellow River basin, which spans 750,000 km^2 and exhibits varied geographical and climatic conditions. The basin's vast scale introduces significant variability in hydrological processes, and the model's 20 km resolution is not well-suited to accurately

Table 1
Experimental Design to Evaluate the Different Sediment Transport Capacity Equations for Overland Flow

		Upland sediment discharge						
Ensemble	Experiments	Description	Rainfall or runoff factor	Slope term	Scaling e_1	Gully factor α	$f_{\text{no-till}}$	K, and P
I	EXP 1	USLE Rainfall	EI_{30}	$20S_0^{1.25}$	38	0.3	0.25	Equation 18 and 1.0
	EXP 2				129	0.2	0.1	
	EXP 3				65	0.3	0.1	
	EXP 4				27	0.4	0.1	
	EXP 5				230	0.0	0.25	
	EXP 6				81	0.2	0.25	
	EXP 7				15	0.4	0.25	
II	EXP 8	KR-1 Runoff	$q^{2.0}$	$S_0^{1.66}$	2.4e4	0.3	0.25	
	EXP 9				1.3e5	0.0	0.25	
	EXP 10				4.7e4	0.2	0.25	
	EXP 11				9.8e3	0.4	0.25	
	EXP 12				7.8e4	0.2	0.1	
	EXP 13				4.1e4	0.3	0.1	
	EXP 14				1.8e4	0.4	0.1	
III	EXP 15	KR-2 Flow	$q^{2.0}$		7.2e6	0.3	0.25	
	EXP 16				3.1e7	0.0	0.25	
	EXP 17				1.3e7	0.2	0.25	
	EXP 18				3.6e6	0.4	0.25	
	EXP 19				1.9e7	0.2	0.1	
	EXP 20				1.1e7	0.3	0.1	
	EXP 21				5.8e6	0.4	0.1	

capture fine-scale daily variations. Monthly calibration effectively averages these variations, focusing on broader spatial and temporal patterns, thus providing a more stable and effective basis for model evaluation. Additionally, hydrological parameters such as riverbed profiles, width-depth relationships, and Manning's coefficients pose representation challenges across this extensive area. Human activities, particularly damming and reservoir operations, significantly affect streamflow and sediment dynamics, with their impacts more appropriately accounted for through monthly calibration. This calibration strategy enhances the reliability and depth of our model evaluations, ensuring that the outputs are both practical and meaningful for assessing the long-term water and sediment budget in the Yellow River basin.

3.4. Evaluation Metrics for Model Performance

The model performance is evaluated by using the following metrics: the Nash–Sutcliffe model efficiency coefficient (NSE) (Nash & Sutcliffe, 1970), Pearson correlation coefficient (Cor), sediment balance index and modified Kling-Gupta efficiency (mKGE). These performance metrics are defined as follows.

$$\text{NSE} = 1.0 - \frac{\sum_{i=1}^{N}\left(P_s^i - P_o^i\right)^2}{\sum_{i=1}^{N}\left(P_o^i - \overline{P_o}\right)^2} \tag{24}$$

$$\text{Cor} = \frac{\sum_{i=1}^{N}\left(P_o^i - \overline{P_o}\right)\left(P_s^i - \overline{P_s}\right)}{\sqrt{\sum_{i=1}^{N}\left(P_s^i - \overline{P_s}\right)^2\left(P_o^i - \overline{P_o}\right)^2}} \tag{25}$$

$$\text{SBI} = \frac{\sum_{i=1}^{N} P_s^i}{\sum_{i=1}^{N} P_o^i} \tag{26}$$

$$\begin{aligned} \text{mKGE} &= 1 - \sqrt{(\text{Cor}-1)^2 + (\lambda-1)^2 + (\gamma-1)^2} \\ \lambda &= \text{bias ratio} = \frac{\mu_S}{\mu_O} \\ \gamma &= \text{variability ratio} = \frac{\sigma_S/\mu_S}{\sigma_O/\mu_O} \end{aligned} \tag{27}$$

where P_s and P_o are the simulated and observed values of the P variable, respectively, and $\overline{P_o}$ is the mean value of P_o, μ_S and μ_O denote the mean of the predicted and observed values, respectively, while σ_S and σ_O denote the corresponding standard deviations.

4. Results

We remark that our work primarily aims to develop a water erosion and sediment transport model for large-scale basins, which can be coupled with land surface and large hydrological models rather than evaluating existing models. To this end, we have revised typical erosion schemes and integrated them into our large-scale hydrological model (AHMS), detailed in Section 2.4. This section presents a comprehensive evaluation of the overall performance of the expanded model.

4.1. Calibration and Validation of the Model

Revised rainfall-based USLE, runoff-based KR and discharge-based KR equations are employed to simulate upland sediment discharge, and their corresponding performances are compared in Figure 5, Figures S5 and S6 in Supporting Information S1. Figure 5 and Table 2 demonstrate that the observed and predicted sediment fluxes for all stations during the calibration and validation periods are quantitatively consistent, including fluctuations and averages, except for the underestimation of sediment fluxes at the TDG station. In particular, excellent agreement between the predictions and observations (mKGE = 0.90, NSE = 0.81) is obtained at the outlet of the middle reaches in the Yellow River Basin (HYK station). The highest accuracy was achieved at the LM and HYK stations, highlighting the critical role of gully erosion on the Loess Plateau, which is discussed in the next section. Consistent with the sediment yield observations in Figure S4 in Supporting Information S1, the simulated sediment fluxes at TNH, LZ and TDG are relatively small compared with their counterparts at LM and HYK, with a maximum peak of approximately 20 ton s^{-1}.

4.2. Impact of Permanent Gully Erosion on Sediment Dynamics

The TDG-LM sub-basin is characterized by significant permanent gully activity and severe concatenated erosion processes, which contribute large amounts of sediment to the Yellow River (Figure 3). To validate the gully area factor, it is necessary to consider the long-term averaged sediment yield predicted by the model for the five sub-basins: HW-TNH, TNH-LZ, LZ-TDG, TDG-LM, and LM-HYK (Sub-basins 1–5).

Figure 6 shows that in the absence of the gully factor, the model underestimates the sediment yields in Sub-basin 4 (TDG-LM), which is characterized by significant permanent gully activity and a high gully density index, and overestimates the sediment yields in permanent gully-free Sub-basins 1, 2 and 5. According to our model results, Sub-basin 3 is identified as an area of net deposition. Comparison with the observed sediment yield suggests that the model underestimates erosion in this area. A more detailed discussion of this observation will be provided in Section 5.3. Figure 7 demonstrates that incorporating the gully factor improves the model's predictions, as the predicted sediment transport capacity of overland flow and net eroded and deposited soils (with positive values indicating erosion) agree well with the observed large permanent gully area (see Figure 3). In contrast, without the gully factor, the model tends to overestimate sediment yield in steep areas (see Figure 4b for slope and Figure 7d).

4.3. Predicting Upland Sediment Discharge Using Rainfall, Runoff and Overland Flow

Table 3 displays the ensemble modeling results for the suspended sediment discharge, considering the three ensembles I, II and III defined in Section 3.3.2, along with corresponding observations at five hydrological stations. The model performance evaluation indicators at the HYK station show the best agreement and stability between simulated and corresponding observed data using USLE rainfall-runoff erosivity (EI_{30}). This best

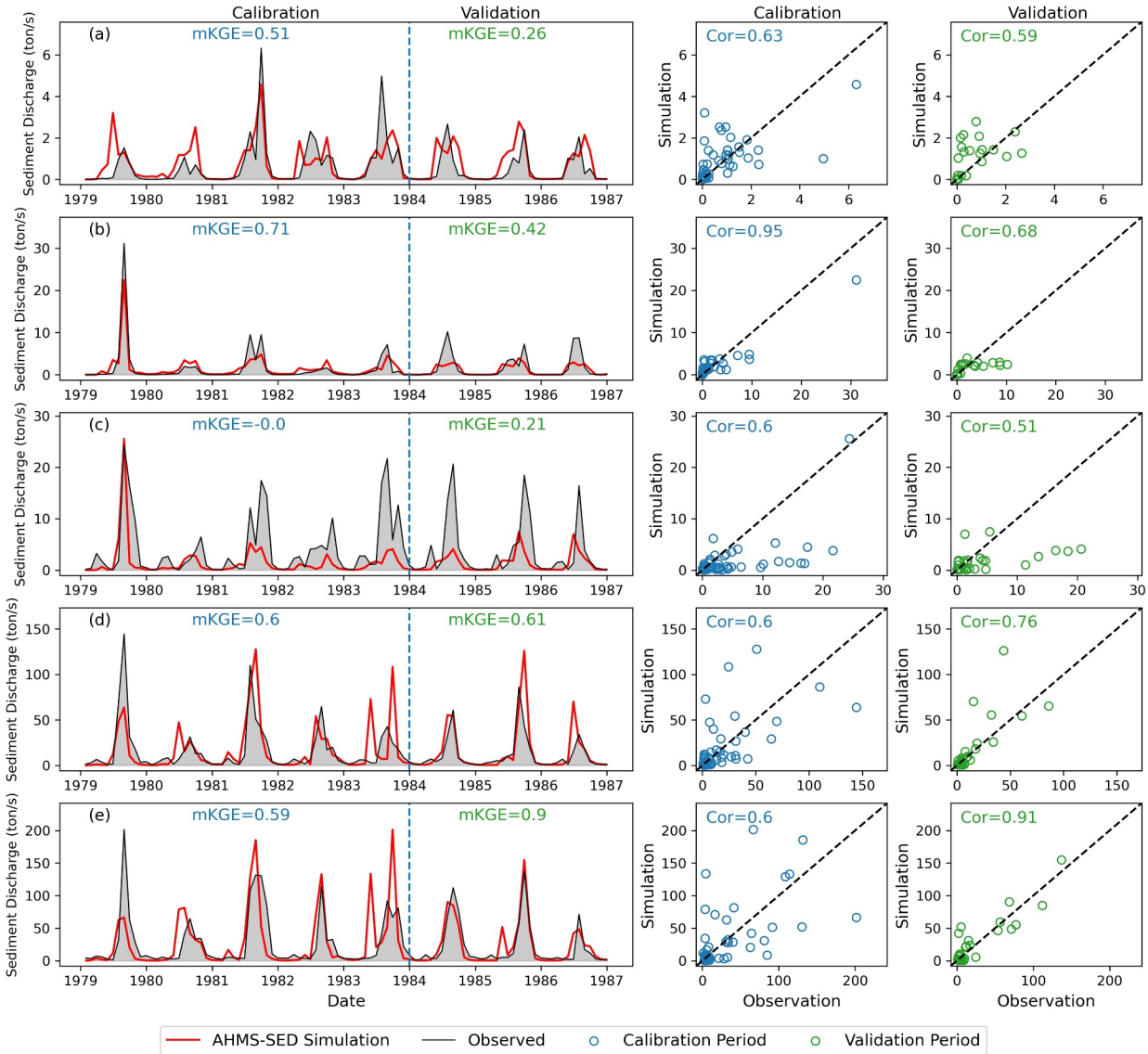

Figure 5. Comparison of observed and predicted monthly suspended sediment discharge at the five hydrological stations: Tangnaihai (a), Lanzhou (b), Toudaoguai (c), Longmen (d) and Huayuankou (HYK) (e). HYK corresponds to the midstream outlet. Results of EXP 1 are shown here, and the upland erosion equation is based on the Universal Soil Loss Equation rainfall erosivity (EI_{30}). The left column presents the time series obtained in the simulations with corresponding observations for comparison, with the dashed line delimiting the calibration (1979–1983) and validation (1984–1986) periods. The middle and right columns show scatter plots for each period, with the 1:1 line in black. Model performance metrics, including modified Kling-Gupta efficiency and correlation (Cor), are provided. Note that the range of the *y*-axis is not the same for the five subplots.

Table 2
Statistical Evaluation for the Suspended Sediment Discharge, Predicted by the Model, Based on Corresponding Observations at Five Hydrological Stations

	Calibration period (1979–1983)					Validation period (1984–1986)				
Stations	Mean obs (Mt a^{-1})	Mean sim (Mt a^{-1})	SBI	mKGE	NSE	Mean obs (Mt a^{-1})	Mean sim (Mt a^{-1})	SBI	mKGE	NSE
TNH	20.6	23.5	1.14	0.51	0.35	14.0	20.4	1.57	0.26	−0.15
LZ	49.9	47.7	0.96	0.71	0.83	53.8	31.3	0.63	0.42	0.35
TDG	127.3	46.0	0.36	−0.00	0.16	109.0	38.0	0.38	0.21	0.08
LM	514.1	517.8	1.01	0.60	0.17	368.1	477.5	1.27	0.61	0.08
HYK	868.5	865.7	1.00	0.59	0.11	666.0	681.7	1.04	0.90	0.81

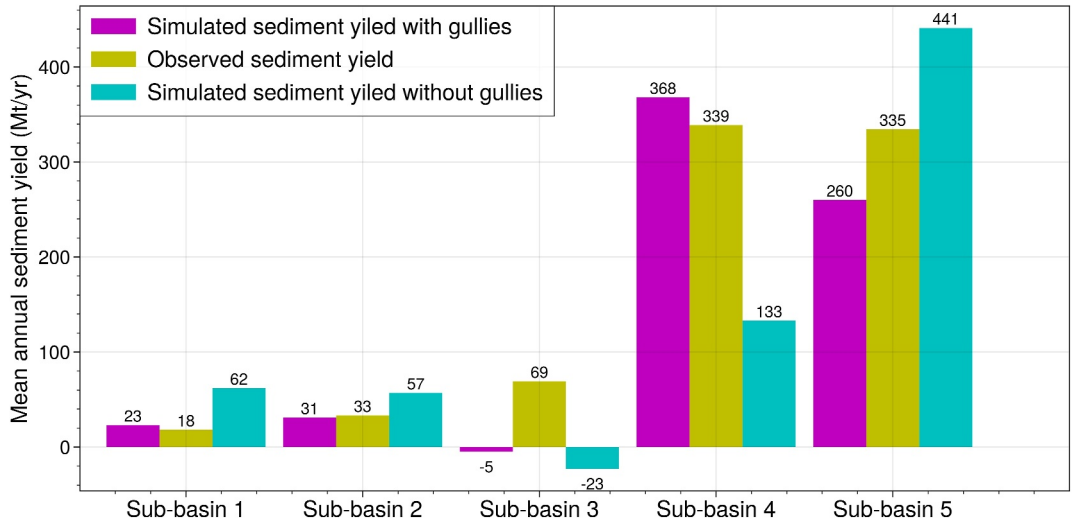

Figure 6. Simulation and corresponding observations of annual mean sediment yield averaged over 1979–1987 in the Yellow River. The simulations with and without the gully factor are EXP 1 and EXP 5.

agreement can be understood by noting that rainfall-runoff erosivity is still the most accurate variable inside large-scale watersheds, while runoff can be predicted more accurately than overland flow.

Specifically, Table 3 and Figure S5 in Supporting Information S1 show that the sediment yields predicted by the KR-runoff equation are overestimated in humid mountainous areas, such as at TNH and LZ, where subsurface runoff significantly contributes to the total runoff. The KR equation performs better in arid and semi-arid regions of the basin. Indeed, in the land surface model (Noah-MP), surface and subsurface runoff are not accurately partitioned in mountainous areas. Figure S6 in Supporting Information S1 shows that the overland flow-based KR equation function performs poorly in the simulation, especially during extreme flood events. Therefore, the inability to accurately simulate surface runoff at the basin scale is a significant limitation of sediment yield models

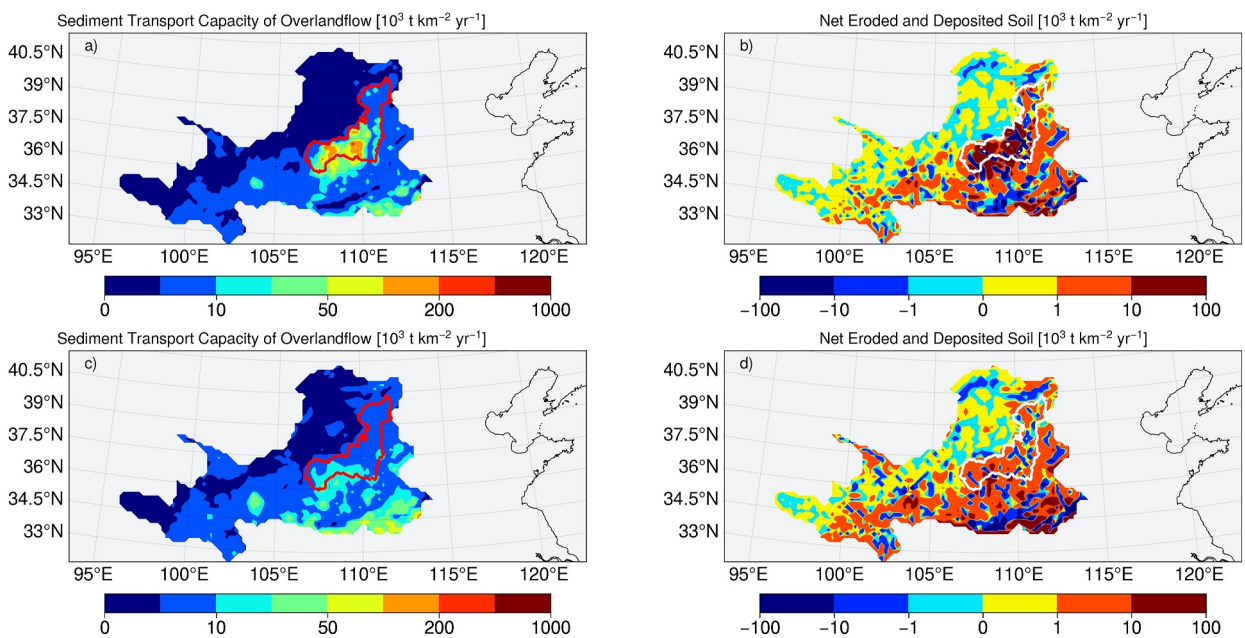

Figure 7. Spatial distribution of offline AHMS-SED simulated annual mean sediment transport capacity of overland flow, net eroded and deposited soil in the Yellow River over 1979–1987. Positive values indicate deposition, while negative values indicate erosion. Subfigures (a) and (b) with the gully factor (EXP 1), while subfigures (c) and (d) without the gully factor (EXP 5).

Table 3
Statistical Evaluation of the Modeling Ensemble Average of Suspended Sediment Discharge Obtained With the Model, Along With Corresponding Observations at Four Hydrological Stations

		Calibration period (1979–1983)					Validation period (1984–1986)				
Stations	Ensemble	Mean obs (Mt a^{-1})	Mean sim (Mt a^{-1})	Mean SBI	Mean mKGE	Mean NSE	Mean obs (Mt a^{-1})	Mean sim (Mt a^{-1})	Mean SBI	Mean mKGE	Mean NSE
TNH	I	20.6	20.43	0.99	0.38	0.22	14.0	19.11	1.37	0.23	−0.29
	II		68.19	3.31	−1.45	−5.90		62.77	4.48	−2.57	−13.94
	III		30.35	1.47	−0.12	−2.48		24.66	1.76	−0.24	−2.96
LZ	I	49.9	45.91	0.92	0.63	0.78	53.8	32.37	0.60	0.37	0.30
	II		119.18	2.39	−0.47	−0.24		96.21	1.79	−0.10	3.26
	III		201.01	4.03	−2.19	−50.39		47.43	0.88	0.20	0.02
TDG	I	127.3	44.13	0.35	−0.10	0.10	109.0	39.42	0.36	0.19	0.06
	II		98.23	0.77	0.33	−0.01		79.21	0.73	0.32	0.22
	III		194.34	1.53	−2.28	−35.80		35.79	0.33	0.04	−0.06
LM	I	514.1	482.40	0.94	0.56	0.16	368.1	435.59	1.18	0.59	−0.03
	II		450.69	0.88	0.51	−0.06		211.66	0.58	0.62	0.30
	III		446.41	0.87	0.10	−0.09		144.79	0.39	0.25	0.13
HYK	I	868.5	868.50	1.00	0.59	0.12	666.0	684.87	1.03	0.85	0.74
	II		861.26	0.99	0.54	−0.02		578.31	0.87	0.68	0.54
	III		869.95	1.00	0.50	−0.01		511.71	0.77	−0.05	−14.10

based on the KR equation. Overall, incorporating the gully factor and USLE rainfall-runoff erosivity (EI_{30}) over a nearly decade-long period yields stable and accurate sediment yields for the entire watershed (Table 3).

4.4. Sensitivity of Sediment Discharge to Climate and Environmental Changes

We conducted a sensitivity test using the AHMS-SED model to assess how variations in climate parameters influence sediment transport and yields in the Yellow River Basin. The historical meteorological data from the 1980s served as the baseline for the model, ensuring robust calibration and validation.

Figure 8 illustrates the insights gained from the sensitivity test, which are as follows:

1. Halving precipitation intensity reduces sediment discharge by 99%, primarily due to the high sensitivity of infiltration-excess runoff generation and upland sediment yield to the rainfall intensity.
2. A 2°C temperature increase slightly reduces sediment yields. While increased temperature affects evapotranspiration and soil moisture, it has minimal impact on sediment transport dynamics directly.
3. Halving precipitation amount decreases sediment discharge by 59%, though its effect is much less significant compared to precipitation intensity.
4. Doubling irrigation reduces sediment discharge by 10%, likely due to reduced streamflow and increased river sediment deposition.

5. Discussions

5.1. Comparison of Gully and Slope Factors

Gully erosion plays a significant role in sediment transport within hydrological basins, particularly in areas with permanent gullies, and its impact increases with spatial scale. This underscores the importance of incorporating gully-related parameters into upland sediment flux models (de Vente & Poesen, 2005; Poesen et al., 1996, 2003). While slope-based models (e.g., Pelletier, 2012; Roering et al., 1999) use strongly nonlinear relationships to capture landslide effects, they may inadequately represent gully erosion dynamics. To address this, we propose the gully area index and gully factor as alternatives, based on dimensional analysis and derived physical equations under idealized assumptions (see Section 2.4.1), offering a more comprehensive approach to erosion modeling.

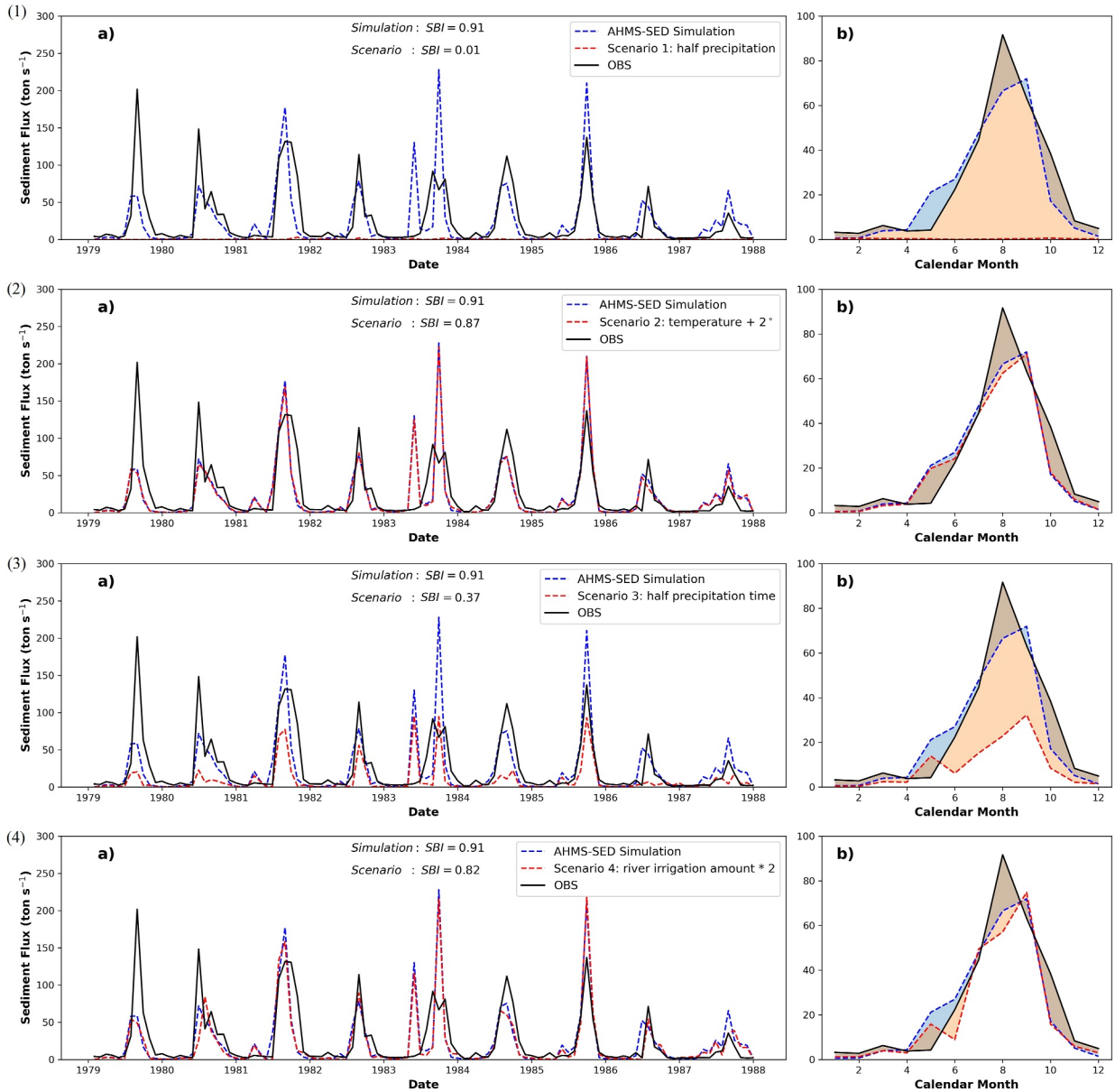

Figure 8. Comparison of (a) monthly and (b) averaged annual cycles of predicted (dashed lines), which is under (red) and not under (blue) specific climate change scenarios (Scenario 1, 2, and 3) and observed (solid line) sediment flux at the outlet of middle reaches of Yellow River Basin (HYK station) for the period of 1979–1987. Subfigure (1) Scenario 1: precipitation halves, which means the precipitation rate is uniformly halved during the study period. Subfigure (2) Scenario 2: temperature rises by 2° evenly during the study period. Subfigure (3) Scenario 3: precipitation time (or amount) is halved, which means no rainfall on the even days (1979.01.02, 1979.01.04, 1979.01.06, …) during the study period. (4) Scenario 4: doubling the amount of river irrigation during the study period.

The Pearson correlation coefficient (Cor) in Figure S7 in Supporting Information S1 reveals a negative linear relationship between the slope factor (S) and the gully area index (G_a) for slopes exceeding 15°. This indicates that gully distribution depends not only on slope but also on factors such as climate, geology, and vegetation. For example, steep mountainous areas such as the Qinghai-Tibet Plateau are characterized by little sediment yields compared to the Loess Plateau in the Yellow River Basin. The variable of the slope is, therefore, not a direct indicator of the intensity of gully erosion. By contrast, the gully area index represents the surface fragmentation, that is, gully area fraction or gully density, and is, thus, a better indicator of gully erosion intensity. Thus, our study demonstrates that gully erosion cannot be adequately represented solely by the slope factor, underscoring the need to incorporate the gully area index for a more comprehensive understanding of sediment transport dynamics.

Previous studies lack robust formulas and data sets on the fraction area of large-scale gullies to effectively characterize gully erosion. The gully area index introduced here provides a novel descriptor of gully erosion and its contribution to sediment sources in catchment-scale hydrological and sediment transport modeling. We propose that the gully area index is an adequate parameter for regional hydrological and sediment transport modeling, as the slope factor used in current models is deficient and suitable only for small-scale systems. Future application and evaluation of the gully area index across diverse watersheds, landforms, and climates will be crucial for advancing regional water erosion and sediment modeling.

5.2. Scaling Challenges and Solutions

Scaling issues arise in any study attempting to model hydrological behavior and related water erosion and sediment transport processes without resolving equations for every hillslope unit (Yu et al., 2006). This study addresses two key scaling issues in large-scale water erosion and sediment transport modeling: (a) downscaling climate forcing timescales from daily or sub-daily to hourly and short durations (b) resolving upland sediment yield at scales with grid cell sizes from 1 km to tens of kilometers.

For the first scaling issue, the 30-min rainfall-runoff erosivity index (EI_{30}) derived from coarse fixed-interval rainfall data is significantly lower than that estimated from breakpoint rainfall data (Panagos et al., 2015; Yin et al., 2007). Following Yin et al. (2007), we calculate the EI_{30} for each hydrology grid cell by scaling the LSM timestep-averaged rainfall rate with a linear scaling parameter that increases with the LSM timestep. Since only fixed-interval rainfall data are available in the LSM, future work could explore incorporating a more advanced probability distribution function to better capture rainfall intensity variability.

Regarding the second scaling issue, the 20 km grid cell size used in this study, while effectively simulating the hydrological and sediment transport processes in the calibration and validation tests (see Section 4.1), is too coarse to resolve individual gullies and hillslopes. The optimal grid scale for predicting water erosion and sediment transport processes remains an open question (Pelletier, 2012; Wood et al., 1988). Parameters associated with topographic variables, such as slope, usually decrease rapidly as grid resolution decreases. Furthermore, a grid cell size of several kilometers may not capture most spatial heterogeneities in rainfall, runoff, and overland flow. To address this, we introduced a linear scaling parameter to account for the decay of slope, rainfall, runoff, or overland flow with decreasing grid resolution. Overall, the scaling parameter e_1 encodes information about rainfall or runoff and slope. However, this scaling-dependent parameter increases as grid resolution decreases. Future studies should explore advanced probability distribution functions to better account for the stochastic properties of runoff, overland flow, or shear stress on the ground.

5.3. Cropland Erosion

According to both the irrigation fraction map (Ozdogan & Gutman, 2008) and the Global Map of Irrigation Areas (Siebert et al., 2005), irrigation is most intensive in Sub-basins 3 and 5. Figure S8 in Supporting Information S1 shows that EXP 3 indicates that a relatively higher amount of cropland erosion in Sub-basin 5 will yield an improved agreement between predicted and observed sediment yield, compared to EXP 1 (see Figure 6). As seen, changing the no-tillage factor causes no significant change in cropland erosion for Sub-basin 3. This behavior is attributed to the underestimation of sediment transport capacity and the flow velocity in the river in this area. Future research should use additional streamflow observations to evaluate river flow velocity, depth, and corresponding sediment transport capacity.

5.4. Sedimentation in Reservoirs

Increasing anthropogenic activities in the Yellow River Basin, such as dams and reservoirs, usually significantly impact the dynamics of suspended sediment load through sedimentation (Wang et al., 2016; Y. Yu et al., 2013). Here, the potential sedimentation by the reservoir is examined by comparing the sediment fluxes at the reservoir's upstream and downstream gauge stations. Figures S9a and S9c in Supporting Information S1 show that the outflow sediment flux at the Longyangxia and Sanmenxia Reservoirs is larger than the inflow sediment flux at the same reservoirs. Therefore, we conclude that sediment flux at these reservoirs did not change substantially from 1979 to 1987. However, as shown in Figure S9b in Supporting Information S1, the outflow sediment flux is slightly lower than the inflow of Liujiaxia Reservoir. Therefore, we propose that sediment flux at the Liujiaxia

Reservoir slightly changed over time due to sedimentation in the reservoir. It would be interesting to extend the AHMS-SED sediment transport model in future work to incorporate the effects of sedimentation in the reservoirs.

5.5. Impacts of Climate Variables on Sediment Discharge

The response of the water cycle and the transport of carbon, nutrients and sediments to climate change constitutes a topic of great interest to the scientific community and has significant implications for society (Chahine, 1992; Schlesinger & Bernhardt, 2020). A growing body of evidence (Allen & Ingram, 2002; Folland et al., 2002; Genfo et al., 1991; Huntington, 2006; Li et al., 2021; Loaiciga et al., 1996; Trenberth, 1999) suggests that climate warming will accelerate the water cycle, leading to changes in precipitation and runoff, and increase the frequency and intensity of extreme hydrological events. These transformations in the water cycle and the concatenated changes in hydrological processes could lead to substantial enhancement of erosion and sediment discharge at the regional scale.

Representing and quantifying the water cycle and the transport of carbon, nutrients, and sediments at a large scale is crucial, as it provides a comprehensive understanding of regional and global biogeochemical processes. This large-scale perspective highlights gaps in our understanding that are often encountered in small-scale simulations. Small-scale studies, while detailed, may not capture the broader interactions and cumulative impacts of climate change on hydrological and sediment transport processes. Thus, large-scale studies are essential to bridge this gap and provide a more holistic view of the changes occurring in these systems.

Predicting climate-change-driven decadal evolution of sediment transport rates at the regional scale is challenging, owing to the broad range of atmospheric, hydrological, anthropogenic and geomorphological variables involved. Indeed, our coupled hydrological-atmospheric simulations incorporate both the effect of irrigation on hydrological processes (Jiang et al., 2022) and a comprehensive module for soil erosion processes at the catchment-scale. To address this complexity, we conducted a sensitivity test in Section 4.4 using the AHMS-SED model to understand how specific variables in climate change and anthropogenic scenarios influence the evolution of sediment yields in the Yellow River Basin. We found that precipitation intensity significantly influences sediment yields, while increased river irrigation reduces sediment transport. This approach helps in isolating the impact of individual factors on sediment transport processes.

We are aware of the limitations of this part of our study, as we only altered one variable at a time rather than fully integrating comprehensive climate and land use changes. Future research should incorporate the latest Intergovernmental Panel on Climate Change scenarios, specifically the Representative Concentration Pathways and Shared Socioeconomic Pathways provided by CMIP5 and CMIP6. The integration of these scenarios into our coupled simulations of hydrological and sediment transport processes would constitute an excellent topic for continuation of the present study in a future work, to elucidate concrete potential scenarios of climate-change-driven sediment transport processes in the Yellow River Basin. Moreover, future studies should be dedicated to validating model predictions with observed data from various regions to investigate the combined effects of multiple climate variables on sediment yields. This would ensure consistency and comparability with other studies.

6. Conclusions and Outlook

Suspended sediment discharge is rarely represented in regional hydrological models. This study investigated whether sediment discharge in large catchments can be reliably quantified using advanced land surface and large-scale hydrological models. To this end, we developed the AHMS-SED model by integrating the Atmospheric and Hydrological-Irrigation Modeling System with the revised CASC2D-SED. This integration allows the model to align with AHMS hydrological processes and incorporate three distinct upland sediment transport capacity equations based on the rainfall, runoff and overland flow. A key achievement of this study is the introduction of the gully area index to quantify erosion enhancement induced by concentrated flow in gullies at regional scales, thus providing a measure of its potential impact on regional sediment supply. We addressed the often-neglected aspects of sediment dynamics which are vital for accurate large-scale sediment modeling.

Specifically, the AHMS-SED model was applied to the Yellow River Basin to simulate water erosion and sediment processes from 1979 to 1987. We found that the AHMS-SED model can accurately predict monthly suspended sediment fluxes at five major hydrological stations in the Yellow River Basin, with strong agreement with observations (mKGE = 0.90, NSE = 0.81 at the basin outlet). The gully area index and sediment transport

capacity of overland flow spatially aligned with observed sediment source hotspots on the Loess Plateau, and incorporating gully erosion significantly improved sediment budget accuracy. We further evaluated various sediment transport equations, examining their effectiveness in capturing upland processes influenced by different hydrological drivers. Among the tested sediment transport equations, the USLE-EI30 proved to be the most effective erosivity predictor for large-scale water erosion, whereas models such as the KR equation, which rely primarily on runoff and overland flow, exhibited limitations in accurately simulating surface runoff at the basin scale. Moroever, a sensitivity analysis was conducted to evaluate how changes in precipitation patterns, temperature, and irrigation practices might influence sediment transport and yields under various climate scenarios. Our results highlight the extreme sensitivity of sediment yields in the Yellow River Basin to precipitation rates, surpassing the influence of precipitation volume, temperature, and river irrigation.

Future research should improve the model by developing a scale-adaptive parameterization for water erosion, reducing dependence on scale-specific parameters, and incorporating stochastic distributions to better capture the heterogeneity of precipitation, runoff, and overland flow. Additionally, integrating a sedimentation model to account for reservoir and dam influences will enhance the model's applicability to a broader range of hydrological conditions. By expanding the calibration data set to include detailed flow velocity and depth measurements, along with a multi-stage calibration approach, further improvement will be achieved in the sediment transport and deposition predictions, particularly in key sub-basins like LZ-TDG.

The AHMS-SED modeling system, which integrates a regional land surface model with a large-scale hydrological model, offers significant potential for improving predictions of suspended sediment flux and sediment yield in large watersheds. These processes are key to global biogeochemical cycles, transporting organic and inorganic carbon, along with nutrients, from terrestrial environments to aquatic ecosystems. At the same time, this research highlights the limitations of current large-scale hydrological models in representing water erosion—especially with respect to erosivity schemes, scaling, and gully erosion. By addressing these gaps, AHMS-SED advances sediment transport modeling and provides a valuable tool for researchers and policymakers. Further refinement and application of AHMS-SED across diverse geographical and climatic contexts will enhance our understanding of large-scale sediment discharge, its impacts on carbon and nutrient cycles, and ultimately strengthen environmental planning and conservation strategies in the face of global climate change.

Conflict of Interest

The authors declare no conflicts of interest relevant to this study.

Data Availability Statement

The Atmospheric and Hydrological-Sediment Modeling System (AHMS-SED) version 1.0, used for simulating hydrological and sediment processes in the study, is preserved at Zenodo via https://doi.org/10.5281/zenodo.14494932 under the CC BY 4.0 license (Jiang, 2024a). Development and updates for AHMS-SED are openly maintained on GitHub at https://github.com/JiangCong1990/AHMS-SED. Additionally, the observation data, model input data, and simulation results of AHMS-SED for the Yellow River Basin used in this study are openly available at Zenodo via https://doi.org/10.5281/zenodo.14983610 under the CC BY 4.0 license (Jiang, 2024b).

Acknowledgments
We thank the German Research Foundation (DFG) for funding through the Heisenberg Programme "Multiscale Simulation of Earth Surface Processes", project number 434377576 and through SFB 1211 "Earth - Evolution at the Dry Limit", project number 268236062. We furthermore thank the Regional Computing Center of the University of Cologne (RRZK) for providing computing time on the DFG-funded (Funding number: INST 216/512/1FUGG) High-Performance Computing system CHEOPS as well as support. We also thank the German Computing Centre (DKRZ, Hamburg) for providing computing time and storage capacities. We sincerely thank the anonymous reviewers for their constructive comments and suggestions, which have significantly improved the quality of this manuscript. We also appreciate the editors for their valuable feedback and professional handling of the review process. Open Access funding enabled and organized by Projekt DEAL.

References

Ali, M., Seeger, M., Sterk, G., & Moore, D. (2013). A unit stream power based sediment transport function for overland flow. *Catena*, *101*, 197–204. https://doi.org/10.1016/j.catena.2012.09.006

Allen, M. R., & Ingram, W. J. (2002). Constraints on future changes in climate and the hydrologic cycle. *Nature*, *419*(6903), 224–232. https://doi.org/10.1038/nature01092

Arnold, J. G., & Fohrer, N. (2005). SWAT2000: Current capabilities and research opportunities in applied watershed modelling. *Hydrological Processes*, *19*(3), 563–572. https://doi.org/10.1002/hyp.5611

Bowling, L. C., Pomeroy, J. W., & Lettenmaier, D. P. (2004). Parameterization of blowing-snow sublimation in a macroscale hydrology model. *Journal of Hydrometeorology*, *5*(5), 745–762. https://doi.org/10.1175/1525-7541(2004)005<0745:POBSIA>2.0.CO;2

Chahine, M. T. (1992). The hydrological cycle and its influence on climate. In *Nature* (Vol. 359(6394). 373–380). https://doi.org/10.1038/359373a0

Chen, L., Li, Y., Chen, F., Barr, A., Barlage, M., & Wan, B. (2016). The incorporation of an organic soil layer in the Noah-MP land surface model and its evaluation over a boreal aspen forest. *Atmospheric Chemistry and Physics*, *16*(13), 8375–8387. https://doi.org/10.5194/acp-16-8375-2016

Chen, Y., Yang, K., Tang, W., Li, X., Lu, H., He, J., & Qin, J. (2015). China meteorological forcing dataset (1979–2018) [Dataset]. *National Tibetan Plateau Data Center*. https://doi.org/10.11888/AtmosphericPhysics.tpe.249369.file

Cuntz, M., Mai, J., Samaniego, L., Clark, M., Wulfmeyer, V., Branch, O., et al. (2016). The impact of standard and hard-coded parameters on the hydrologic fluxes in the Noah-MP land surface model. *Journal of Geophysical Research*, *121*(18), 10676–10700. https://doi.org/10.1002/2016JD025097

Davis, R. O. E., & Bennett, H. H. (1927). Grouping of soils on the basis of mechanical analysis. *419*, 1–15.

De Geeter, S., Verstraeten, G., Poesen, J., Campforts, B., & Vanmaercke, M. (2023). A data driven gully head susceptibility map of Africa at 30 m resolution. *Environmental Research*, *224*, 115573. https://doi.org/10.1016/j.envres.2023.115573

de Vente, J., & Poesen, J. (2005). Predicting soil erosion and sediment yield at the basin scale: Scale issues and semi-quantitative models. *Earth-Science Reviews*, *71*(1), 95–125. https://doi.org/10.1016/j.earscirev.2005.02.002

de Vente, J., Poesen, J., Verstraeten, G., Govers, G., Vanmaercke, M., Van Rompaey, A., et al. (2013). Predicting soil erosion and sediment yield at regional scales: Where do we stand? *Earth-Science Reviews*, *127*, 16–29. https://doi.org/10.1016/j.earscirev.2013.08.014

Dietrich, W. E., Bellugi, D. G., Sklar, L. S., Stock, J. D., Heimsath, A. M., & Roering, J. J. (2003). Geomorphic transport laws for predicting landscape form and dynamics. In *Prediction in Geomorphology* (pp. 103–132). American Geophysical Union (AGU). https://doi.org/10.1029/135GM09

Einstein, H. A. (1964). River sedimentation. In *Handbook of Applied Hydrology, Section--17*.

Engelund, F., & Hansen, E. (1967). A monograph on sediment transport in alluvial streams. *Monografia*.

Fagundes, H. O., Fan, F. M., Paiva, R. C. D., Siqueira, V. A., Buarque, D. C., Kornowski, L. W., et al. (2021). Sediment flows in south America supported by daily hydrologic-hydrodynamic modeling. *Water Resources Research*, *57*(2), 1–26. https://doi.org/10.1029/2020WR027884

FAO. (1991). The digitized soil map of the world (release 1.0). In *World Soil Resources Report 67/1*.

Farr, T. G., Rosen, P. A., Caro, E., Crippen, R., Duren, R., Hensley, S., et al. (2007). The shuttle radar topography mission. *Reviews of Geophysics*, *45*(2). https://doi.org/10.1029/2005RG000183

Folland, C. K., Karl, T. R., & Jim Salinger, M. (2002). Observed climate variability and change. *Weather*, *57*(8), 269–278. https://doi.org/10.1256/004316502320517353

Gao, P., Geissen, V., Ritsema, C. J., Mu, X.-M., & Wang, F. (2013). Impact of climate change and anthropogenic activities on stream flow and sediment discharge in the Wei River basin, China. *Hydrology and Earth System Sciences*, *17*(3), 961–972. https://doi.org/10.5194/hess-17-961-2013

Genfo, A. D. D., Lacis, A. A., & Ruedy, R. A. (1991). Simulations of the effect of a warmer climate on atmospheric humidity. *Nature*, *351*(6325), 382–385. https://doi.org/10.1038/351382a0

Govers, G. (1990). *Empirical relationships for the transport capacity of overland flow* (Vol. 189, pp. 45–63). IAHS Publication.

Hajigholizadeh, M., Melesse, A. M., & Fuentes, H. R. (2018). Erosion and sediment transport modelling in shallowwaters: A review on approaches, models and applications. *International Journal of Environmental Research and Public Health*, *15*(3), 518. https://doi.org/10.3390/ijerph15030518

Harmon, R. S., Doe III, W. W., & Doe, W. W. (2001). *Landscape erosion and evolution modelling*. Springer Science and Business Media.

Hassan, M. A., Church, M., Xu, J., & Yan, Y. (2008). Spatial and temporal variation of sediment yield in the landscape: Example of Huanghe (Yellow River). *Geophysical Research Letters*, *35*(6), L06401. https://doi.org/10.1029/2008GL033428

He, C., Valayamkunnath, P., Barlage, M., Chen, F., Gochis, D., Cabell, R., et al. (2023). Modernizing the open-source community Noah with multi-parameterization options (Noah-MP) land surface model (version 5.0) with enhanced modularity, interoperability, and applicability. *Geoscientific Model Development*, *16*(17), 5131–5151. https://doi.org/10.5194/gmd-16-5131-2023

He, J., Yang, K., Tang, W., Lu, H., Qin, J., Chen, Y., & Li, X. (2020). The first high-resolution meteorological forcing dataset for land process studies over China. *Scientific Data*, *7*(1), 1–11. https://doi.org/10.1038/s41597-020-0369-y

Hessel, R., & Jetten, V. (2007). Suitability of transport equations in modelling soil erosion for a small Loess Plateau catchment. *Engineering Geology*, *91*(1), 56–71. https://doi.org/10.1016/j.enggeo.2006.12.013

Hessel, R., Jetten, V., Baoyuan, L., Yan, Z., & Stolte, J. (2003). Calibration of the LISEM model for a small Loess Plateau catchment. *Catena*, *54*(1–2), 235–254. https://doi.org/10.1016/S0341-8162(03)00067-5

Huntington, T. G. (2006). Evidence for intensification of the global water cycle: Review and synthesis. *Journal of Hydrology*, *319*(1–4), 83–95. https://doi.org/10.1016/j.jhydrol.2005.07.003

Irannejad, P., & Shao, Y. (1998). Description and validation of the atmosphere-land-surface interaction scheme (ALSIS) with HAPEX and Cabauw data. *Global and Planetary Change*, *19*(1–4), 87–114. https://doi.org/10.1016/S0921-8181(98)00043-5

Jakeman, A. J., Green, T. R., Beavis, S. G., Zhang, L., Dietrich, C. R., & Crapper, P. F. (1999). Modelling upland and instream erosion, sediment and phosphorus transport in a large catchment. *Hydrological Processes*, *13*(5), 745–752. https://doi.org/10.1002/(SICI)1099-1085(19990415)13:5<745::AID-HYP777>3.0.CO;2-E

Jiang, C. (2024a). Atmospheric and hydrological-sediment modelling system (AHMS-SED) [Software]. *Zenodo*. https://doi.org/10.5281/zenodo.14494932

Jiang, C. (2024b). Observation data, model input data, and simulation results for the Yellow River Basin [Dataset]. *Zenodo*. https://doi.org/10.5281/zenodo.14983610

Jiang, C., Parteli, E. J. R., Xia, Q., & Shao, Y. (2024). Evaluation of precipitation reanalysis products for regional hydrological modelling in the Yellow River Basin. *Theoretical and Applied Climatology*, *155*(4), 2605–2626. https://doi.org/10.1007/s00704-023-04758-w

Jiang, C., Parteli, E. J. R., Xia, Q., Yin, X., & Shao, Y. (2022). A regional hydrological model for arid and semi-arid river basins with consideration of irrigation. *Environmental Modelling & Software*, *157*, 105531. https://doi.org/10.1016/j.envsoft.2022.105531

Johnson, B. E. (1997). *Development of a storm-event-based two-dimensional upland erosion model (sediment yield)*. Colorado State University.

Jordan, R. (1991). *A one-Dimensional Temperature Model for a snow Cover: Technical Documentation for SNTHERM.89*. U.S.Army Corps of Engineers, Cold Regions Research and Engineering Laboratory.

Jpl, N. (2013). NASA shuttle Radar topography mission global 1 arc second. *NASA EOSDIS Land Processes Distributed Active Archive Center*. https://doi.org/10.5067/MEaSUREs/SRTM/SRTMGL1.003

Julien, P. Y. (2010). *Erosion and sedimentation*. Cambridge University Press.

Julien, P. Y., Saghafian, B., & Ogden, F. L. (1995). Raster-based hydrologic modeling of spatially-varied surface runoff. *JAWRA Journal of the American Water Resources Association*, *31*(3), 523–536. https://doi.org/10.1111/j.1752-1688.1995.tb04039.x

Julien, P. Y., & Simons, D. B. (1984). Analysis of sediment transport equations for rainfall erosion. *Civil Engineering Department, Engineering Research Center, Colorado State∼…*.

Julien, P. Y., & Simons, D. B. (1985). Sediment transport capacity of overland flow. *Transactions of the ASAE*, *28*(3), 755–762. https://doi.org/10.13031/2013.32333

Kilinc, M. Y. (1972). *Mechanics of soil erosion from overland flow generated by simulated rainfall*. Colorado State University. Retrieved from https://www.proquest.com/dissertations-theses/mechanics-soil-erosion-overland-flow-generated/docview/302680155/se-2

Kilinc, M. Y., & Richardson, E. V. (1973). Mechanics of soil erosion from overland flow generated by simulated rainfall. *Colo State Univ (Fort Collins), Hydrol Papers*, *63*.
Kinnell, P. I. A. (2005). Raindrop-impact-induced erosion processes and prediction: A review. *Hydrological Processes*, *19*(14), 2815–2844. https://doi.org/10.1002/hyp.5788
Kinnell, P. I. A., & Risse, L. M. (1998). USLE-M: Empirical modeling rainfall erosion through runoff and sediment concentration. *Soil Science Society of America Journal*, *62*(6), 1667–1672. https://doi.org/10.2136/sssaj1998.03615995006200060026x
Lal, R. (2003). Soil erosion and the global carbon budget. In *Environment International* (Vol. 29(4). 437–450). https://doi.org/10.1016/S0160-4120(02)00192-7
Lal, R. (2017). Soil erosion by wind and water: Problems and prospects. In *Soil erosion Research Methods*. https://doi.org/10.1201/9780203739358
Lane, L. J., Hernandez, M., & Nichols, M. (1997). Processes controlling sediment yield from watersheds as functions of spatial scale. *Environmental Modelling & Software*, *12*(4), 355–369. https://doi.org/10.1016/S1364-8152(97)00027-3
Largeron, C., Cloke, H. L., Verhoef, A., Martinez-de-la-Torre, A., & Mueller-Quintino, A. (2018). Impact of the representation of the infiltration on the river flow during intense rainfall events in Jules. *ECMWF Technical Memoranda, January*. https://www.ecmwf.int/node/18245
Leopold, L. B., & Maddock, T. Jr. (1953). The hydraulic geometry of stream channels and some physiographic implications. In *Geological Survey Professional Paper 252*.
Li, D., Lu, X., Overeem, I., Walling, D. E., Syvitski, J., Kettner, A. J., et al. (2021). Exceptional increases in fluvial sediment fluxes in a warmer and wetter High Mountain Asia. *Science*, *374*(6567), 599–603. https://doi.org/10.1126/science.abi9649
Li, Y., Poesen, J., Yang, J. C., Fu, B., & Zhang, J. H. (2003). Evaluating gully erosion using 137Cs and 210Pb/137Cs ratio in a reservoir catchment. *Soil and Tillage Research*, *69*(1–2), 107–115. https://doi.org/10.1016/S0167-1987(02)00132-0
Li, Z., Zhang, Y., Zhu, Q., Yang, S., Li, H., & Ma, H. (2017). A gully erosion assessment model for the Chinese Loess Plateau based on changes in gully length and area. *Catena*, *148*, 195–203. https://doi.org/10.1016/j.catena.2016.04.018
Loaiciga, H. A., Valdes, J. B., Vogel, R., Garvey, J., & Schwarz, H. (1996). Global warming and the hydrologic cycle. *Journal of Hydrology*, *174*(1–2), 83–127. https://doi.org/10.1016/0022-1694(95)02753-X
Ludwig, W., Probst, J. L., & Kempe, S. (1996). Predicting the oceanic input of organic carbon by continental erosion. *Global Biogeochemical Cycles*, *10*(1), 23–41. https://doi.org/10.1029/95GB02925
Lukey, B. T., Bathurst, J. C., Hiley, R. A., & Ewen, J. (1995). SHETRAN sediment transport component: equations and algorithms (pp. 1–54).
Maetens, W., Vanmaercke, M., Poesen, J., Jankauskas, B., Jankauskiene, G., & Ionita, I. (2012). Effects of land use on annual runoff and soil loss in Europe and the mediterranean: A meta-analysis of plot data. *Progress in Physical Geography*, *36*(5), 599–653. https://doi.org/10.1177/0309133312451303
Mao, D., Cherkauer, K. A., & Flanagan, D. C. (2010). Development of a coupled soil erosion and large-scale hydrology modelling system. *Water Resources Research*, *46*(8), 1–15. https://doi.org/10.1029/2009WR008268
Merritt, W. S., Letcher, R. A., & Jakeman, A. J. (2003). A review of erosion and sediment transport models. *Environmental Modelling & Software*, *18*(8–9), 761–799. https://doi.org/10.1016/S1364-8152(03)00078-1
Montgomery, D. R. (2007). Soil erosion and agricultural sustainability. *Proceedings of the National Academy of Sciences*, *104*(33), 13268–13272. https://doi.org/10.1073/pnas.0611508104
Morgan, R. P. C., Morgan, D. D. V., & Finney, H. J. (1984). A predictive model for the assessment of soil erosion risk. *Journal of Agricultural Engineering Research*, *30*(C), 245–253. https://doi.org/10.1016/S0021-8634(84)80025-6
Morgan, R. P. C., & Nearing, M. A. (2011). Handbook of erosion modelling. In *Handbook of Erosion Modelling*. https://doi.org/10.1002/9781444328455
Morgan, R. P. C., Quinton, J. N., Smith, R. E., Govers, G., Poesen, J. W. A., Auerswald, K., et al. (1998). The European soil erosion model (EUROSEM): A dynamic approach for predicting sediment transport from fields and small catchments. *Earth Surface Processes and Landforms*, *23*(6), 527–544. https://doi.org/10.1002/(SICI)1096-9837(199806)23:6<527::AID-ESP868>3.0.CO;2-5
Nash, E., & Sutcliffe, V. (1970). River flow forecasting through conceptual models part I. A discussion of principles. *Journal of Hydrology*, *10*(3), 282–290. https://doi.org/10.1016/0022-1694(70)90255-6
Nearing, M. A. (2000). Comments on "USLE-M: Empirical modelling rainfall erosion through runoff and sediment concentration.". *Soil Science Society of America Journal*, *64*(3), 1137.
Neitsch, S. L., Arnold, J. G., Kiniry, J. R., & Williams, J. R. (2011). Soil and water assessment tool theoretical documentation version 2009.
Newbold, T., Hudson, L. N., Hill, S. L. L., Contu, S., Lysenko, I., Senior, R. A., et al. (2015). Global effects of land use on local terrestrial biodiversity. *Nature*, *520*(7545), 45–50. https://doi.org/10.1038/nature14324
Niu, G., Yang, Z. L., Mitchell, K. E., Chen, F., Ek, M. B., Barlage, M., et al. (2011). The community Noah land surface model with multi-parameterization options (Noah-MP): 1. *Evaluation over Global River Basins, Journal of Geophysical Research: Atmospheres*, *116*, 12. https://doi.org/10.1029/2010JD015139
Oost, K. Van, Quine, T. A., Govers, G., Gryze, S. D., Six, J., Harden, J. W., et al. (2007). The impact of agricultural soil erosion on the global carbon cycle. *Science*, *318*(5850), 626–629. https://doi.org/10.1126/science.1145724
Ozdogan, M., & Gutman, G. (2008). A new methodology to map irrigated areas using multi-temporal MODIS and ancillary data: An application example in the continental US. *Remote Sensing of Environment*, *112*(9), 3520–3537. https://doi.org/10.1016/j.rse.2008.04.010
Panagos, P., Ballabio, C., Borrelli, P., Meusburger, K., Klik, A., Rousseva, S., et al. (2015). Rainfall erosivity in Europe. *Science of the Total Environment*, *511*, 801–814. https://doi.org/10.1016/j.scitotenv.2015.01.008
Pelletier, J. D. (2012). A spatially distributed model for the long-term suspended sediment discharge and delivery ratio of drainage basins. *Journal of Geophysical Research*, *117*(F2). https://doi.org/10.1029/2011JF002129
Poesen, J., Nachtergaele, J., Verstraeten, G., & Valentin, C. (2003). Gully erosion and environmental change: Importance and research needs. *Catena*, *50*(2), 91–133. https://doi.org/10.1016/S0341-8162(02)00143-1
Poesen, J. W., Vandaele, K., & Van Wesemael, B. (1996). *Contribution of gully erosion to sediment production on cultivated lands and rangelands* (Vol. 236, pp. 251–266). IAHS Publications-Series of Proceedings and Reports-Intern Assoc Hydrological Sciences.
Qian, N., & Dai, D. Z. (1980). The problems of river sedimentation and the present status of its research in China. *Proceedings of the International Symposium on River Sedimentation*, *24*(29), 19–39.
Renard, K. G., Laflen, J. M., Foster, G. R., & McCool, D. K. (2017). The revised universal soil loss equation. In *Soil erosion research methods* (pp. 105–126). Routledge.
Rijn, L. C. van. (1986). Mathematical modelling of suspended sediment in nonuniform flows. *Journal of Hydraulic Engineering*, *112*(6), 433–455. https://doi.org/10.1061/(asce)0733-9429(1986)112:6(433)

Roering, J. J., Kirchner, J. W., & Dietrich, W. E. (1999). Evidence for nonlinear, diffusive sediment transport on hillslopes and implications for landscape morphology. *Water Resources Research*, *35*(3), 853–870. https://doi.org/10.1029/1998WR900090

Rojas, R., Julien, P., & Johnson, B. (2003). A 2-dimensional rainfall-runoff and sediment model. *CASC2D-SED Reference Manual v1. 0*.

Rojas, S. R. (2002). *GIS-based upland erosion modelling, geovisualization and grid size effects on erosion simulations with CASC2D-SED*. Colorado State University.

Schlesinger, W. H., & Bernhardt, E. (2020). Biogeochemistry: An analysis of global change. In *Biogeochemistry: An Analysis of Global Change*. https://doi.org/10.1016/B978-0-12-814608-8.09991-6

Shangguan, W., Dai, Y., Liu, B., Ye, A., & Yuan, H. (2012a). 30 arc-seconds resolution soil particle-size distribution dataset for regional land and climate modelling in China [Dataset]. *Land-Atmosphere Interaction Research Group, Sun Yat-sen University*. http://globalchange.bnu.edu.cn/research/soil

Shangguan, W., Dai, Y., Liu, B., Ye, A., & Yuan, H. (2012b). A soil particle-size distribution dataset for regional land and climate modelling in China. *Geoderma*, *171–172*, 85–91. https://doi.org/10.1016/j.geoderma.2011.01.013

Shi, H., & Shao, M. (2000). Soil and water loss from the Loess Plateau in China. *Journal of Arid Environments*, *45*(1), 9–20. https://doi.org/10.1006/jare.1999.0618

Siebert, S., Döll, P., Hoogeveen, J., Faures, J. M., Frenken, K., & Feick, S. (2005). Development and validation of the global map of irrigation areas. *Hydrology and Earth System Sciences*, *9*(5), 535–547. https://doi.org/10.5194/hess-9-535-2005

Soil Survey Division Staff. (1993). *Soil survey manual*. US Department of Agriculture.

Stewart, J. R., Livneh, B., Kasprzyk, J. R., Rajagopalan, B., Minear, J. T., & Raseman, W. J. (2017). A Multialgorithm approach to land surface modeling of suspended sediment in the Colorado Front range. *Journal of Advances in Modeling Earth Systems*, *9*(7), 2526–2544. https://doi.org/10.1002/2017MS001120

Syvitski, J. P. M., Vorosmarty, C. J., Kettner, A. J., & Green, P. (2005). Impact of humans on the flux of terrestrial sediment to the global coastal ocean. *Science*, *308*(5720), 376–380. https://doi.org/10.1126/science.1109454

Tan, Z., Leung, L. R., Li, H. Y., & Tesfa, T. (2017). Modeling sediment yield in land surface and Earth system models: Model comparison, development, and evaluation. *Journal of Advances in Modeling Earth Systems*, *10*(9), 2192–2213. https://doi.org/10.1029/2017MS001270

Tan, Z., Leung, L. R., Li, H. Y., & Tesfa, T. (2018). Modeling sediment yield in land surface and Earth system models: Model comparison, development, and evaluation. *Journal of Advances in Modeling Earth Systems*, *10*(9), 2192–2213. https://doi.org/10.1029/2017MS001270

Trenberth, K. E. (1999). Conceptual framework for changes of extremes of the hydrological cycle with climate change. *Climatic Change*, *42*(1), 327–339. https://doi.org/10.1023/A:1005488920935

Tucker, G. E., & Hancock, G. R. (2010). Modelling landscape evolution. *Earth Surface Processes and Landforms*, *35*(1), 28–50. https://doi.org/10.1002/esp.1952

Vanoni, V. A. (2006). Sedimentation engineering (classic Ed). *American Society of Civil Engineers*. https://doi.org/10.1061/9780784408230

Van Rompaey, A., Verstraeten, G., Van Oost, K., Rozanov, A., Govers, G., & Poesen, J. (2001). Modelling sediment transport in the Jonkershoek catchment Part 1: Model calibration and validation. In *Modelling Sediment Transport in the Jonkershoek Catchment Part 1: Model Calibration and Validation*.

Vigiak, O., Malagó, A., Bouraoui, F., Vanmaercke, M., Obreja, F., Poesen, J., et al. (2017). Modelling sediment fluxes in the Danube River Basin with SWAT. *Science of the Total Environment*, 599–600. https://doi.org/10.1016/j.scitotenv.2017.04.236

Wang, S., Fu, B., Piao, S., Lü, Y., Ciais, P., Feng, X., & Wang, Y. (2016). Reduced sediment transport in the Yellow River due to anthropogenic changes. *Nature Geoscience*, *9*(1), 38–41. https://doi.org/10.1038/ngeo2602

Ward, R. C., & Robinson, M. (1975). *Principles of hydrology* (Vol. 367). McGraw-Hill.

Wilkinson, B. H., & McElroy, B. J. (2007). The impact of humans on continental erosion and sedimentation. *Bulletin of the Geological Society of America*, *119*(1–2), 140–156. https://doi.org/10.1130/B25899.1

Wischmeier, W. H., & Smith, D. D. (1978). Predicting rainfall erosion losses: A guide to conservation planning *(issue 537)*. Department of Agriculture, Science and Education Administration.

Wood, E. F., Sivapalan, M., Beven, K., & Band, L. (1988). Effects of spatial variability and scale with implications to hydrologic modelling. *Journal of Hydrology*, *102*(1–4), 29–47. https://doi.org/10.1016/0022-1694(88)90090-X

Wu, Y., & Cheng, H. (2005). Monitoring of gully erosion on the Loess Plateau of China using a global positioning system. *Catena*, *63*(2–3), 154–166. https://doi.org/10.1016/j.catena.2005.06.002

Xia, Q. (2019). Development and application of a coupled atmospheric and hydrological modelling system. https://kups.ub.uni-koeln.de/9450/.1–125.

Xu, J. (1999). Erosion caused by hyperconcentrated flow on the Loess Plateau of China. *Catena*, *36*(1–2), 1–19. https://doi.org/10.1016/S0341-8162(99)00009-0

Yamazaki, D., Ikeshima, D., Sosa, J., Bates, P. D., Allen, G. H., & Pavelsky, T. M. (2019a). MERIT hydro: A high-resolution global hydrography map based on latest topography dataset. *Water Resources Research*, *55*(6), 5053–5073. https://doi.org/10.1029/2019WR024873

Yamazaki, D., Ikeshima, D., Sosa, J., Bates, P. D., Allen, G. H., & Pavelsky, T. M. (2019b). Multi-error-removed improved-terrain DEM (MERIT DEM) [Dataset]. *The University of Tokyo*. http://hydro.iis.u-tokyo.ac.jp/~yamadai/MERIT_DEM/

Yang, K., He, J., Tang, W., Lu, H., Qin, J., Chen, Y., & Li, X. (2015). China meteorological forcing dataset (1979-2018). In *National Tibetan plateau Data Center*. National Tibetan Plateau Data Center. https://doi.org/10.11888/AtmosphericPhysics.tpe.249369.file

Yellow River Basin Monitoring Center. (2020). The boundary data of the high and coarse sediment yield in the middle Yellow River [Dataset]. *National Cryosphere Desert Data Center of China*. https://doi.org/10.12072/ncdc.HHSBJC.db0001.2020

Yin, S., Xie, Y., Nearing, M. A., & Wang, C. (2007). Estimation of rainfall erosivity using 5- to 60-minute fixed-interval rainfall data from China. *Catena*, *70*(3), 306–312. https://doi.org/10.1016/j.catena.2006.10.011

Yu, Y., Wang, H., Shi, X., Ran, X., Cui, T., Qiao, S., & Liu, Y. (2013). New discharge regime of the Huanghe (Yellow River): Causes and implications. *Continental Shelf Research*, *69*, 62–72. https://doi.org/10.1016/j.csr.2013.09.013

Yu, Z., Lakhtakia, M. N., Yarnal, B., White, R. A., Miller, D. A., Frakes, B., et al. (1999). Simulating the river-basin response to atmospheric forcing by linking a mesoscale meteorological model and hydrologic model system. *Journal of Hydrology*, *218*(1–2), 72–91. https://doi.org/10.1016/S0022-1694(99)00022-0

Yu, Z., Pollard, D., & Cheng, L. (2006). On continental-scale hydrologic simulations with a coupled hydrologic model. *Journal of Hydrology*, *331*(1–2), 110–124. https://doi.org/10.1016/j.jhydrol.2006.05.021

Yue, T., Yin, S., Xie, Y., Yu, B., & Liu, B. (2022). Rainfall erosivity mapping over mainland China based on high-density hourly rainfall records. *Earth System Science Data*, *14*(2), 665–682. https://doi.org/10.5194/essd-14-665-2022

Zhang, K., Li, S., Peng, W., & Yu, B. (2004). Erodibility of agricultural soils on the Loess Plateau of China. *Soil and Tillage Research*, *76*(2), 157–165. https://doi.org/10.1016/j.still.2003.09.007

Zheng, F., & Wang, B. (2014). Soil Erosion in the Loess Plateau Region of China. In A. Tsunekawa, G. Liu, N. Yamanaka, & S. Du (Eds.), *Restoration and Development of the Degraded Loess Plateau, China* (pp. 77–92). Springer. https://doi.org/10.1007/978-4-431-54481-4_6

References From the Supporting Information

Abrahams, A. D., Li, G., Krishnan, C., & Atkinson, J. F. (2001). A sediment transport equation for interrill overland flow on rough surfaces. *Earth Surface Processes and Landforms*, *26*(13), 1443–1459. https://doi.org/10.1002/esp.286

Arnold, J. G., Srinivasan, R., Muttiah, R. S., & Williams, J. R. (1998). Large area HYDROLOGIC MODELING and assessment part I: Model DEVELOPMENT1. *JAWRA Journal of the American Water Resources Association*, *34*(1), 73–89. https://doi.org/10.1111/j.1752-1688.1998.tb05961.x

Bagnold, R. A. (1966). *An Approach to the Sediment Transport Problem from General Physics*. USGS Professional Paper.

Bagnold, R. A. (1980). Empirical Correlation of Bedload Transport Rates in Flumes and Natural Rivers. In *Proceedings of The Royal Society of London, Series A: Mathematical and Physical Sciences* (Vol. 372(1751), pp. 453–473). https://doi.org/10.1098/rspa.1980.0122

Ball, J. T., Woodrow, I. E., & Berry, J. A. (1987). A Model Predicting Stomatal Conductance and its Contribution to the Control of Photosynthesis under Different Environmental Conditions. In *Progress in Photosynthesis Research* (pp. 221–224). Springer. https://doi.org/10.1007/978-94-017-0519-6_48

Bicknell, B. R., Imhoff, J. C., Kittle, J. L., Jr., Donigan, A. S., Jr., & Johanson, R. C. (1997). Hydrological Simulation Program--Fortran, User's manual for version 11: U.S. Environmental Protection Agency. In *National Exposure Research Laboratory*. EPA/600/R-97/080.755.

Brutsaert, W. (1981). Evaporation into the atmosphere. Theory, history, and applications. In *Evaporation into the atmosphere. Theory, history, and applications* (Vol. 1). Springer Science \and Business Media. https://doi.org/10.1029/eo063i051p01223-04

Bussi, G., Rodríguez-Lloveras, X., Francés, F., Benito, G., Sánchez-Moya, Y., & Sopeña, A. (2013). Sediment yield model implementation based on check dam infill stratigraphy in a semiarid Mediterranean catchment. *Hydrology and Earth System Sciences*, *17*(8), 3339–3354. https://doi.org/10.5194/hess-17-3339-2013

Chen, F., & Dudhia, J. (2001). Coupling and advanced land surface-hydrology model with the Penn State-NCAR MM5 modelling system. Part I: Model implementation and sensitivity. *Monthly Weather Review*, *129*(4), 569–585. https://doi.org/10.1175/1520-0493(2001)129<0569:CAALSH>2.0.CO;2

De Roo, A. P. J., Wesseling, C. G., & Ritsema, C. J. (1996). LISEM: A single-event physically based hydrological and soil erosion model for drainage basins. I: Theory, input and output. *Hydrological Processes*, *10*(8), 1107–1117. https://doi.org/10.1002/(SICI)1099-1085(199608)10:8<1107::AID-HYP415>3.0.CO;2-4

DuBoys, M. P. (1879). Le Rhône et les rivières à lit affouillable. *Annals de Ponts et Chaussée*, *18*(5), 141–195.

Eekhout, J. P. C., Jódar-Abellán, A., Carrillo-López, E., Boix-Fayos, C., & de Vente, J. (2024). Assessing the hillslope-channel contributions to the catchment sediment balance under climate change. *Environmental Modelling & Software*, *171*, 105890. https://doi.org/10.1016/j.envsoft.2023.105890

Everaert, W. (1991). Empirical relations for the sediment transport capacity of interrill flow. *Earth Surface Processes and Landforms*, *16*(6), 513–532. https://doi.org/10.1002/esp.3290160604

Ewen, J., Parkin, G., & O'Connell, P. E. (2000). SHETRAN: Distributed River Basin Flow and Transport Modeling System. *Journal of Hydrologic Engineering*, *5*(3), 250–258. https://doi.org/10.1061/(ASCE)1084-0699(2000)5:3(250)

Govers, G. (1992). Evaluation of transporting capacity formulae for overland flow. *Overland Flow Hydraulics and Erosion Mechanics*, 243–273.

Laflen, J. M., Lane, L. J., & Foster, G. R. (1991). WEPP: A new generation of erosion prediction technology. *Journal of Soil and Water Conservation*, *46*(1), 34–38.

Lazar, A. N., Butterfield, D., Futter, M. N., Rankinen, K., Thouvenot-Korppoo, M., Jarritt, N., et al. (2010). An assessment of the fine sediment dynamics in an upland river system: INCA-Sed modifications and implications for fisheries. *Science of the Total Environment*, *408*(12), 2555–2566. https://doi.org/10.1016/j.scitotenv.2010.02.030

Nearing, M. A., Norton, L. D., Bulgakov, D. A., Larionov, G. A., West, L. T., & Dontsova, K. M. (1997). Hydraulics and erosion in eroding rills. *Water Resources Research*, *33*(4), 865–876. https://doi.org/10.1029/97WR00013

Nearing, M. A., Wei, H., Stone, J. J., Pierson, F. B., Spaeth, K. E., Weltz, M. A., et al. (2011). A rangeland hydrology and erosion model. *Transactions of the ASABE*, *54*(3), 901–908. https://doi.org/10.13031/2013.37115

Niu, G. Y., & Yang, Z. L. (2006). Effects of frozen soil on snowmelt runoff and soil water storage at a continental scale. *Journal of Hydrometeorology*, *7*(5), 937–952. https://doi.org/10.1175/JHM538.1

Nunes, J. P., Vieira, G. N., Seixas, J., Gonçalves, P., & Carvalhais, N. (2005). Evaluating the MEFIDIS model for runoff and soil erosion prediction during rainfall events. *Catena*, *61*(2–3), 210–228. https://doi.org/10.1016/j.catena.2005.03.005

Sellers, P. J., Dickinson, R. E., Randall, D. A., Betts, A. K., Hall, F. G., Berry, J. A., et al. (1997). Modeling the exchanges of energy, water, and carbon between continents and the atmosphere. In *Science* (Vol. 275(5299), 502–509). https://doi.org/10.1126/science.275.5299.502

Smart, G. M. (1984). Sediment Transport Formula for Steep Channels. *Journal of Hydraulic Engineering*, *110*(3), 267–276. https://doi.org/10.1061/(asce)0733-9429(1984)110:3(267)

Stokes, G. G. (1851). On the effect of the Internal friction of fluids on the motion of pendulums - Section III. *Transactions of the Cambridge Philosophical Society*, *IX*, 1–10.

Trimble, S. W., & Crosson, P. (2000). U.S. soil erosion rates - Myth and reality. In *Science* (Vol. 289(5477), 248–250). https://doi.org/10.1126/science.289.5477.248

Verseghy, D. L. (1991). Class—A Canadian land surface scheme for GCMS. I. Soil model. *International Journal of Climatology*, *11*(2), 111–133. https://doi.org/10.1002/joc.3370110202

Wicks, J. M., & Bathurst, J. C. (1996). SHESED: A physically based, distributed erosion and sediment yield component for the SHE hydrological modelling system. *Journal of Hydrology*, *175*(1–4), 213–238. https://doi.org/10.1016/S0022-1694(96)80012-6

Yalin, M. S. (1963). An Expression for Bed-Load Transportation. *Journal of the Hydraulics Division*, *89*(3), 221–250. https://doi.org/10.1061/JYCEAJ.0000874

Yang, C. T. (1972). Unit Stream Power and Sediment Transport. *Journal of the Hydraulics Division*, *98*(10), 1805–1826. https://doi.org/10.1061/JYCEAJ.0003439

Yang, C. T. (1973). Incipient motion and sediment transport. *ASCE J Hydraul Div*, *99*(HY10), 1679–1704. https://doi.org/10.1061/jyceaj.0003766